

Local Nucleosome Dynamics Facilitate Chromatin Accessibility in Living

Mammalian Cells

Saera Hihara

Doctor of Philosophy

Biological Macromolecule Laboratory, Structural Biology Center

National Institute of Genetics

Department of Genetics, School of Life Science

The Graduate University for Advanced Studies

2012 (School Year)

CONTENTS

1. ABSTRACT.....	1
2. INTRODUCTION.....	6
2-1. Genomic DNA.....	6
2-2. Nucleosome.....	6
2-3. A novel insight into chromatin structure.....	7
2-4. Chromatin dynamics.....	9
2-5. Aim and achievement of this research.....	10
3. RESULTS.....	12
3-1. FCS Measurements of Interphase Chromatin and Mitotic Chromosomes in Living Cells.....	12
3-2. Interphase Chromatin and Mitotic Chromosomes Exhibit Comparable Protein Diffusibility.....	13
3-3. Nucleosome Concentrations within Interphase Nuclei and Mitotic Chromosomes.....	15
3-4. Reconstruction of the Chromatin Environment Using Metropolis Monte Carlo Simulations.....	15
3-5. Nucleosome Fluctuation Facilitates Protein Diffusibility in Dense Chromatin Regions.....	17
3-6. Single Nucleosome Imaging in Living Cells.....	17
3-7. Local Nucleosome Fluctuation in Living Cells.....	18
3-8. Inhibition of the Local Nucleosome Dynamics Impaired Targeting Efficiency in Dense Chromatin Regions.....	21
4. DISCUSSION.....	22
5. FIGURES AND FIGURE LEGENDS.....	26
6. EXPERIMENTAL PROCEDURES.....	64
7. ACKNOWLEDGEMENTS.....	76
8. REFERENCES.....	77

LIST OF FIGURES

Figure 1. Chromatin structure.....	26
Figure 2. Novel chromatin structure model based on the polymer melt hypothesis.....	27
Figure 3. Schematic diagram of FCS measurement.....	29
Figure 4. The cell line suitable for inspecting the chromosome environment.....	30
Figure 5. Indian Muntjac and Indian Muntjac cell (DM cell) chromosomes.....	31
Figure 6. Schematic representation of introduction of the constructs into the Indian Muntjac (DM Cell) genome.....	32
Figure 7. DM cell lines expressing EGFP-monomer, trimer, and pentamer.....	33
Figure 8. Photobleaching of H2B-mRFP1 after FCS measurement.....	34
Figure 9. Verification of proper expression of EGFP-monomer, trimer, and pentamer (Left) and H2B-mRFP1 (Right).....	35
Figure 10. Photobleaching of H2B-mRFP1 after FCS measurement in living cells.....	36
Figure 11. Normalized fluorescence autocorrelation functions (FAFs) of the EGFP-trimer in living interphase (Black Line) and mitotic (Red Line) cells.....	37
Figure 12. Mean values of diffusion coefficients (D_s).....	38

Figure 13. Measurements of nucleosome concentrations in interphase nuclei and mitotic chromosomes.....	40
Figure 14. Reconstructions of the living chromatin environment by Metropolis Monte Carlo Computer Simulations.....	42
Figure 15. The trajectories of the diffusing green balls (EGFP-pentamer molecules) in fixed red ball environments.....	43
Figure 16. The trajectories of the diffusing green balls in fluctuated red ball environment.....	44
Figure 17. Terminal diffusion coefficients (D_s) of green balls with various nucleosome concentrations, which were fixed (Red) or fluctuated (Green).....	45
Figure 18. Terminal D_s of the green balls with 0.5 mM red balls and various “dog leash” lengths (maximum displacement of nucleosomes).....	46
Figure 19. Structural integrity of nucleosomes containing PA-GFP-H4.....	47
Figure 20. Photoactivation of PA-GFP-H4 in the DM Cells.....	49
Figure 21. Nuclear image of DM cells expressing PA-GFP-H4.....	50
Figure 22. Single-step photobleaching of PA-GFP-H4 dots.....	51
Figure 23. Displacement (movement) distributions of single nucleosomes.....	52
Figure 24. Plots of the mean square displacements (MSDs) of single nucleosomes for 30, 60, and 90 ms in interphase chromatin (A) and mitotic chromosomes (B).....	53

Figure 25. Centroid movements of a number of observed nucleosomes.....	55
Figure 26. Single nucleosome movement in formaldehyde-fixed cells.....	56
Figure 27. Movement of single fluorescence beads (A) ($n = 100$) and cross-linked nucleosomes in glutaraldehyde-fixed cells (B) ($n = 8$).....	57
Figure 28. Schematic representation of the experiment.....	58
Figure 29. Tight cross-linking of nucleosomes blocks antibody accessibility and targeting.....	59
Figure 30. Detection of CAP-H2 signals by Western blotting of cell lysates, which were fixed with glutaraldehyde on the membrane.....	61
Figure 31. Slower diffusion of EGFP-monomer molecules in apoptotic chromatin.....	62
Figure 32. The dynamic local movement of nucleosomes.....	63

1. ABSTRACT

In cell nuclei or mitotic chromosomes, long strings of genomic DNA are organized three-dimensionally to perform genome functions during cellular proliferation, differentiation, and development. The DNA is wrapped around histones, forming a nucleosome structure. The nucleosome had been assumed to be folded into a 30-nm chromatin fiber and other helical folding structures. However, recent studies, including our cryo-microscopy (cryo-EM) and synchrotron X-ray scattering analyses, have shown almost no visible 30-nm chromatin fibers or other regular structures in interphase nuclei and mitotic chromosomes. This suggests that chromosomes consist of irregularly folded nucleosome fibers comprising a polymer melt-like structure. Thus, nucleosome fibers may be constantly moving and rearranging at the local level. These local nucleosome dynamics could be crucial for various genome functions.

I studied the dynamic aspects of nucleosomes in living cells. Because the dynamic chromatin environment in living cells is difficult to study using traditional fluorescence and electron microscopy, I used, with the help of my collaborators, a combination of fluorescence correlation spectroscopy (FCS), single molecule imaging, and Metropolis Monte Carlo computer simulations.

First, to determine the chromatin environment in living cells, I employed FCS using free enhanced green fluorescent proteins (EGFPs). FCS detects the Brownian motion of free EGFPs in a small detection volume based on fluorescence intensity fluctuations and provides the diffusion coefficient (D) of the EGFPs, which indicates how far the molecules can move in a particular time. Thus, D gives useful information on their environment, with a smaller D indicating that the molecule exists in a more crowded environment, and vice versa. I measured D s of EGFP-monomer, -trimer, or -pentamer molecules in interphase chromatin and mitotic chromosomes. Unexpectedly, D in mitotic chromosomes was quite comparable to that in interphase chromatin, thus suggesting that protein mobility in interphase chromatin and that the mitotic chromosome is comparable.

Next, based on the physical parameters obtained via FCS, the chromatin environment *in silico* was reconstructed using the Metropolis Monte Carlo method to simulate EGFP behavior under various chromatin conditions. To simulate the diffusion of EGFP pentamers from the Stokes–Einstein relation, I represented EGFP-pentamer molecules as 13-nm-diameter green balls. Nucleosomes were represented as 10-nm-diameter red balls and fixed in a space at a concentration of 0.1 or 0.5 mM. The 0.5-mM condition

corresponded to mitotic chromosomes and likely interphase heterochromatin. In the environment with 0.1-mM red balls under a fixed condition, the green balls moved around quite freely. However, with 0.5-mM fixed red balls, which represented a dense heterochromatin or chromosome environment, green balls could not move far from their starting position and were trapped in a confined space. Although this simulation suggested that EGFP pentamers in fixed chromatin environments cannot move around freely, it was inconsistent with FCS measurements in the living chromatin environment, in which the apparently free diffusion of EGFP pentamers was observed.

To determine the conditions that could recapitulate the observations *in vivo*, next a simulation with fluctuating red balls was performed. Each red ball acted like “a dog on a leash,” being set in random motion within a certain distance range from the origin. In this dynamic chromatin environment, the green balls appeared to diffuse freely, even with 0.5-mM red balls. Strikingly, a 20-nm maximum displacement of red balls was sufficient for green balls to diffuse freely in the chromatin environment. This finding suggests that the dynamic fluctuation of nucleosomes facilitates the free diffusion of proteins in a compact chromatin environment, such as that in mitotic chromosomes, as well as dense heterochromatin.

An obvious next question was whether the nucleosome fluctuations predicted by the simulation occur in living cells. Therefore, I performed single-particle imaging of nucleosomes in living cells. I fused photoactivatable (PA)-GFP with histone H4, which is a stable core histone component, and then expressed the fusion protein in cells at a very low level. For single nucleosome imaging, I used highly inclined and laminated optical sheet (HILO) microscopy. Unexpectedly, I found that a very small number of PA-GFP-H4s in the stable cells spontaneously activated without laser activation and could be observed as dots. With this imaging system, I recorded nucleosome signals in interphase chromatin and mitotic chromosomes at a video rate of ~ 30 ms/frame as a movie. The averaged displacements (movements) in 30 ms in interphase chromatin and mitotic chromosomes were 51 and 59 nm, respectively, and showed a similar fluctuation in both interphase and mitotic chromatin. Since the displacements of fluorescent beads on the glass surface or in cross-linked nucleosomes in glutaraldehyde-fixed cells were much smaller than those observed in living cells, I concluded that the majority of the displacement came from the movement of nucleosomes in living cells, and not from the drift of the microscopy system.

Last, I examined whether local nucleosome dynamics drive chromatin accessibility or

targeting in dense chromatin regions. To do so, I used immunostaining of condensin in mitotic chromosomes as a model system in dense chromatin regions. Immunostaining signals demonstrated that the antibodies (150 kDa, >15 nm) targeted the condensin complexes in the chromosome axes. Although I detected antibody signals in the chromosome axes of non-fixed cells, far fewer were observed in glutaraldehyde-fixed cells. This finding is consistent with the previous results and indicates that tight cross-linking of nucleosomes blocks antibody accessibility and targeting.

In this study, I showed that interphase chromatin and dense mitotic chromosomes have comparable protein diffusibility. In both chromatins, I observed a novel local dynamics of individual nucleosomes (~50 nm movement/30 ms) caused by Brownian motion. The inhibition of this local dynamics by cross-linking impaired diffusibility and targeting efficiency in dense chromatin regions. I propose that this local movement of nucleosomes is the basis for scanning genome information.

2. INTRODUCTION

2-1. Genomic DNA

The human body consists of 60 trillion cells, each of which contains 2 m of genomic DNA in the nucleus and has a diameter of $\sim 10 \mu\text{m}$ (Figure 1). The genomic DNA encodes genetic information, which is three-dimensionally organized within cells and is searched and read out by various proteins to exert diverse functions within cells. During mitosis, the genomic DNA is compacted into mitotic chromosomes with a diameter of $\sim 700 \text{ nm}$ (Figure 1). This chromosome structure is physically essential for the faithful transmission of duplicated genomic DNA into the two daughter cells during cell division. Organization of the genomic DNA drastically changes during cell cycle, and thus an understanding of how the genomic DNA is packaged in interphase nuclei or mitotic chromosomes is important.

2-2. Nucleosome

DNA has a negatively charged phosphate backbone that produces electrostatic repulsion between adjacent DNA regions, making it difficult for DNA to fold upon itself (Bloomfield 1996; Yoshikawa and Yoshikawa 2002). For folding, a long DNA molecule with a diameter of 2 nm is wrapped around the core histone octamer, which consists of the histone H2A, H2B, H3, and H4 proteins (Kornberg and Lorch 1999), and forms a

nucleosome structure. The structural details of the nucleosome core are now known at a resolution of 1.9 Å (Davey *et al.* 2002). In the nucleosome core particle, 147 bp of DNA is wrapped in 1.7 left-handed superhelical turns around the histone octamer. Each nucleosome core is connected by linker DNA. Therefore, the nucleosome fibers were originally described as “beads on a string” (Olins and Olins 2003). Although the core histones have tails with positively charged lysine and arginine residues, only ~60% of the negative charges of the DNA molecule are neutralized (Strick *et al.* 2001). Consequently, for further folding, the remaining ~40% of the DNA charge must be neutralized by other factors, such as linker histone H1 proteins or cations.

2-3. A novel insight into chromatin structure

For further packaging, the nucleosome was first assumed to be folded into a 30-nm chromatin fiber and further regular helical folding structures (Figure 1) (Alberts *et al.*, 2007). The first evidence regarding the structure of the 30-nm chromatin fiber was gained using conventional transmission (Finch and Klug, 1976; Woodcock *et al.*, 1984). However, for conventional electron microscopic observation, chemical fixation and alcohol dehydration of the sample is inevitable, which could result in the generation of

artificial fiber structures (Maeshima *et al.*, 2010b). So, what does chromatin in fact look like in living cells?

One of the best ways to approach this question is by using cryo-microscopy of vitreous sections (CEMOVIS). Cryo-microscopy (cryo-EM) is based on “vitrification” by rapid cooling, which ensures immobilization of all macromolecules in the sample in a close-to-native state (Frank, 2006). After the samples are sectioned, the thin vitrified sections are directly observed under a cryo-EM without any chemical fixation or staining. This approach enables direct, high-resolution imaging of cell structures in a close-to-native state.

Recent evidence, including our recent cryo-EM and synchrotron X-ray scattering analyses, showed almost no visible 30-nm chromatin fibers or further regular structures in mitotic chromosomes (Figure 2A) (Eltsov *et al.*, 2008; Maeshima *et al.*, 2010a; Nishino *et al.*, 2012), which suggests that chromosomes consist of irregularly folded nucleosome fibers with a fractal organization, *i.e.*, a polymer melt-like structure. More recently, an absence of 30-nm chromatin fibers in the majority of active interphase cells was also proposed (Maeshima *et al.*, 2010a; Fussner *et al.*, 2011). The concept of a polymer melt-like structure implies that the nucleosome fibers may be constantly moving and rearranging at the local level, which is likely crucial for various genome

functions involved in most cellular activities (Figure 2B) (Eltsov *et al.*, 2008; Maeshima *et al.*, 2010a; Nishino *et al.*, 2012).

2-4. Chromatin dynamics

Two fluorescence microscopy methods can be used to investigate chromatin dynamics in living cells. The first is fluorescence recovery after photobleaching (FRAP). In FRAP, the part of the cell that is expressing the fluorescence-tagged protein is irradiated with an intense laser pulse to bleach the fluorophore (For review, see Wachsmuth *et al.*, 2008). If all molecules are fixed, the bleached area remains bleached and the unbleached area is unaffected. In contrast, if all molecules are free to diffuse, the fluorescence in the bleached area recovers rapidly to almost the original level. The diffusion rate can be determined by analyzing the recovery kinetics.

The second is the Lac Operator/Repressor system. Multiple copies of the Lac Operator sequence are inserted into a genomic site and the Lac Repressor-fused GFP can bind the region of the Lac Operator to the genomic site, which is observed as a GFP focus (Robinett *et al.*, 1996). By tracking this focus, one can analyze large-scale chromatin movement and dynamics. Although these methods are widely used to

investigate chromatin dynamics, local nucleosome movements, which I described above, may be occur on a smaller scale and thus be inaccessible by these methods.

2-5. Aim and achievement of this research

The aim of my project is to elucidate the local dynamic properties of chromatin in living mammalian cells. Studying the chromatin environment in living cells using traditional fluorescence and electron microscopy is problematic. Thus, I utilized a combined approach of fluorescence correlation spectroscopy (FCS), single molecule imaging, and Metropolis Monte Carlo computer simulations. FCS detects the fluorescence intensity fluctuations caused by Brownian motion of fluorescence probe molecules in a small detection volume generated by confocal microscopic illumination (Gorisch et al., 2005; Pack et al., 2006; Wachsmuth et al., 2008; Bancaud et al., 2009; Dross et al., 2009). Single molecule imaging can reveal the dynamics of specific molecules of interest (Wachsmuth et al., 2008; Levi and Gratton, 2008; Bancaud et al., 2009). Computer simulation enables prediction of the behavior of molecules under conditions that are either difficult to generate experimentally or observe directly using microscopy techniques (Morelli and ten Wolde, 2008). I first observed that interphase chromatin and mitotic chromosomes have comparable protein diffusibilities. I found

novel local dynamics of individual nucleosomes in both chromatins, which drive protein diffusibility and chromatin accessibility in mammalian living cells. The biological significance of these local dynamics is discussed.

3. RESULTS

3-1. FCS Measurements of Interphase Chromatin and Mitotic Chromosomes in Living Cells

To characterize the chromatin accessibility in living cells, I first employed FCS using free EGFPs. Through time correlation analysis of the fluorescence fluctuations (Figure 3), the diffusion coefficient (D) of free EGFPs, which shows how far the molecules can move in a particular time, was obtained (see Experimental Procedures; also see Figure 11). The D of molecules provides useful information on their environment: a smaller D indicates that the molecule exists in a more crowded environment.

However, two problems were encountered with FCS measurements, when analyzing mitotic chromosomes. First, the diameter of FCS detection regions ($\sim 0.4 \mu\text{m}$ diameter \times $\sim 1\text{--}2 \mu\text{m}$ height) is larger than the diameter of typical mammalian chromosomes [$\sim 0.7 \mu\text{m}$ (Alberts *et al.*, 2007)](Figure 4A), which makes specific measurements inside chromosomes difficult. Second, since chromosomes dynamically move and a single FCS measurement takes more than several seconds, I have to confirm that the measured region was actually inside the dynamic chromosomes throughout the recording period. To resolve the first problem, I used an Indian Muntjac cell line (DM cells) (Figure 5) (Manders *et al.*, 1999). DM cells have giant chromosomes whose diameter is much

larger than that of the FCS detection regions (Figure 4B). For the second problem, histone H2B-mRFP1 was co-expressed as a marker of chromatin regions (Dross *et al.*, 2009; Bancaud *et al.*, 2009) (Figure 6 and Figure 7). Upon photobleaching of immobilized H2B-mRFP1 after FCS, the actual measured regions could be identified by confocal imaging, thus avoiding off-target measurements (Figure 8).

To establish DM cell lines stably expressing H2B-mRFP1 and EGFP, I introduced a single copy construct into the DM cell genome by site-specific recombination (Figure 6). To examine the effect of the size of molecules on diffusion, I also generated DM cell lines expressing EGFP-trimers and pentamers with molecular weights of 90 and 150 kDa, respectively (Figures 7 and 9). Multiple oligomeric EGFPs with different molecular weights could be used as molecular rulers for quantifying protein mobility (Pack *et al.*, 2006; Dross *et al.*, 2009; Bancaud *et al.*, 2009). Their proper expression and localization were confirmed by microscopic imaging (Figure 7) and Western blotting (Figure 9).

3-2. Interphase Chromatin and Mitotic Chromosomes Exhibit Comparable Protein Diffusibility

I then measured movement of the EGFP-monomer, trimer, or pentamer molecules in

the interphase chromatin and mitotic chromosomes (Figure 7; see Experimental Procedures). Before and after FCS measurements, cell images were acquired to verify the actual measured regions by photobleaching of H2B-mRFP1 (Figure 10). Based on the measured fluorescence correlation functions, which were well fitted by the one-component model, I calculated the D s of EGFP-monomer, -trimer, or -pentamer molecules (Figure 11; also see Experimental Procedures). Figure 12A shows the D s of monomer EGFP molecules in the cytoplasm, interphase chromatin, and mitotic chromosomes. The D s obtained in the cytoplasm and interphase chromatin are similar to those in previous reports (Pack *et al.*, 2006; Bancaud *et al.*, 2009; Dross *et al.*, 2009). In the mitotic chromosome, apparent protein diffusibility or accessibility was detected, as partly suggested by other procedures (Chen *et al.*, 2005; Hinde *et al.*, 2011; Gorisch *et al.*, 2005).

The D in mitotic chromosomes was only 30% lower than that in interphase chromatin. Since the D is proportional to the square root of molecule displacement (movement) per unit time, the difference in EGFP displacement between interphase and mitotic chromatin was ~18%. I observed similar profiles in the case of EGFP-trimer and pentamer molecules (Figures 12B and Figure 12C). These results suggest that protein mobility in the interphase chromatin and mitotic chromosome is quite comparable.

3-3. Nucleosome Concentrations within Interphase Nuclei and Mitotic Chromosomes

Although large differences in protein diffusibility between interphase chromatin and mitotic chromosomes were not detected, how crowded is the chromatin environment therein? Thus, I examined their nucleosome concentrations. Nuclear and mitotic chromosome volumes in DM cells were measured from their three-dimensional (3D) image stacks (Figures 13A and 13B). Their nucleosome concentrations were calculated based on the measured volumes and the known genome size of Indian Muntjac cells (DM cells) (2.1 pg/haploid genome) (Johnston *et al.*, 1982). The nucleosome concentration in mitotic chromosomes (~0.5 mM) was five-fold higher than that in interphase nuclei (~0.1 mM) (Figure 13C), consistent with previous reports (Wachsmuth *et al.*, 2008), although one must consider that nucleosomes are not evenly distributed within interphase nuclei (See Discussion).

3-4. Reconstruction of the Chromatin Environment Using Metropolis Monte Carlo Simulations

Based on the physical parameters obtained above, the chromatin environment was reconstructed *in silico* using the Metropolis Monte Carlo method (Morelli and ten

Wolde, 2008) to simulate EGFP behavior under various chromatin conditions. To simulate the diffusion of EGFP-pentamers, from the Stokes–Einstein relation, EGFP-pentamer molecules were represented as green balls with a 13 nm diameter (Figure 14; for details, see Experimental Procedures). The nucleosomes were represented as red balls with a diameter of 10 nm and fixed in a space at a concentration of 0.1 or 0.5 mM (Figure 14). The 0.5 mM condition corresponds to mitotic chromosomes and likely interphase heterochromatin (Wachsmuth *et al.*, 2008). In the environment with 0.1 mM red balls under a fixed condition, the green balls moved around quite freely (Figure 15 left and Figure 17). However, with 0.5 mM fixed red balls, which is reminiscent of the dense heterochromatin or chromosome environment, green balls could not move far from their starting position and were trapped in a confined space (Figure 15 right and Figure 17). This simulation suggests that EGFP-pentamers in fixed chromatin environments cannot move around freely. This is inconsistent with the FCS measurements in the living chromatin environment, in which apparently free diffusion of EGFP-pentamers was observed.

3-5. Nucleosome Fluctuation Facilitates Protein Diffusibility in Dense Chromatin

Regions

To determine the conditions that recapitulate the observation *in vivo*, we next performed the simulation with fluctuated red balls. Each red ball acts like “a dog on a leash”: each red ball was set in random motion in a certain distance range from the origin. In this dynamic chromatin environment, apparently free diffusion of green balls was observed even with 0.5 mM red balls (Figure 16 and Figure 17). Strikingly, a 20 nm maximum displacement of nucleosomes was sufficient for EGFP-pentamers to diffuse freely in the chromatin environment (Figure 18). This finding suggests that dynamic fluctuation of nucleosomes facilitates free diffusion of proteins in a compact chromatin environment, such as that in mitotic chromosomes, as well as dense heterochromatin (Wachsmuth *et al.*, 2008).

3-6. Single Nucleosome Imaging in Living Cells

An obvious important question is whether the nucleosome fluctuations predicted by the simulation occur in living cells. Therefore, I performed single particle imaging of nucleosomes in living cells. Fluorescently labeling only a small number of the nucleosomes among $\sim 3 \times 10^7$ in a single nucleus was technically challenging. I fused

photoactivatable (PA)-GFP with histone H4 (Lippincott-Schwartz and Patterson, 2009; Wiesmeijer *et al.*, 2008), which is a stable core histone component (Kimura and Cook, 2001), and then expressed the fusion protein in DM cells at a very low level. Expression and photoactivation of PA-GFP-H4 in stable DM cells were verified by Western blotting (Figure 19A) and 405-nm laser stimulation (Figure 20), respectively. Biochemical fractionation of purified bulk nucleosomes confirmed that the expressed PA-GFP-H4 behaved in a manner similar to endogenous H4 and that the PA-GFP-H4 was properly incorporated into the nucleosome structure (Figure 19B).

For single nucleosome imaging, I used highly inclined and laminated optical sheet (HILO) microscopy (Tokunaga *et al.*, 2008). Unexpectedly, I found that a very small number of PA-GFP-H4 in the stable DM cells was spontaneously activated without laser activation and were observed as dots (Figure 21). Single-step photobleaching of these dots (Figure 22) revealed that each represented a single PA-GFP-H4 molecule in a single nucleosome, allowing one to observe the movement of individual nucleosomes (Figure 21).

3-7. Local Nucleosome Fluctuation in Living Cells

With this imaging system, nucleosome signals in the interphase chromatin and

mitotic chromosomes were recorded at a video-rate (~30 ms/frame) as a movie. The signal particles in each image frame were fitted to an assumed Gaussian point spread function to determine the precise center of signals with a higher resolution below the diffraction limit (Figure 21) (Lippincott-Schwartz and Patterson, 2009). After the position of the signal particles was obtained in every frame of the movie, its trajectory was analyzed as the displacement (movement) (Figure 23) and mean square displacement (MSD) (Figure 24). Since I aimed to examine local nucleosome fluctuations, I analyzed the behavior of nucleosomes within very short time periods: 30, 60, and 90 ms (Figures 23).

Figure 23 shows the displacement distribution of single nucleosomes in living interphase and mitotic cells. The averaged displacements during 30 ms in interphase chromatin and mitotic chromosomes were 51 and 59 nm, respectively. Since the displacements of fluorescent beads on the glass surface or the cross-linked nucleosomes in the glutaraldehyde-fixed cells were much smaller than those observed in living cells (Figure 27), the results indicate that the majority of the displacement came from movement of nucleosomes in living cells, and not drift of the microscopy system. To further exclude the possibility that the detected movement was derived from global motion of the nuclei or chromosomes, movements of the centroid for nucleosomes were

measured and plotted (Figure 25). Since these values were much smaller than the movements of individual nucleosomes in living cells (Figure 23), I concluded that the observed displacement was due to local movement (fluctuation) of nucleosomes in living cells.

To further analyze local nucleosome movement, the displacement of cross-linked nucleosomes in glutaraldehyde-fixed cells was subtracted as background noise from that in living cells, and MSD of the nucleosomes in interphase chromatin and mitotic chromosomes was plotted (Figure 24). The plots were fitted with a linear function formula (thick line), which does not pass through the origin, supporting the restricted nucleosome movement model (see Discussion).

When I used formaldehyde, which less frequently cross-link the same amino acid residues (mainly arginine and lysine) than glutaraldehyde (Griffiths, 1993), I found that the cells still showed considerable nucleosome mobility (50 nm/60 ms) (Figure 26). This result shows that the local nucleosome movement is caused by Brownian motion (see Discussion).

3-8. Inhibition of the Local Nucleosome Dynamics Impaired Targeting Efficiency in Dense Chromatin Regions

Next, I examined whether the local dynamics drive chromatin accessibility or targeting in the dense chromatin regions. To do so, I used immunostaining of condensin (Hirano, 2005) in mitotic chromosomes as a model system in dense chromatin regions. Immunostaining signals demonstrated that the antibodies (150 kDa, >15 nm; Sandin *et al.*, 2004) targeted the condensin complexes in the chromosome axes (Figure 28). I detected antibody signals in the chromosome axes of non- and formaldehyde-fixed cells, but much less was observed in glutaraldehyde-fixed cells (Figure 29). This result is consistent with the previous results (Figure 26 and Figure 27) and shows that tight cross-linking of nucleosomes blocks antibody accessibility and targeting. Since I readily detected by Western blotting the antibody signals in cell lysates which were fixed on the membrane by glutaraldehyde (Figure 30), glutaraldehyde was unlikely to have changed the antibody-epitope(s) and prevented antibody access. This finding supports the idea that local nucleosome movement is important for chromatin accessibility and targeting in dense chromatin regions, which is in good agreement with the results obtained by computer simulation (Figure 15 and Figure 16) and single nucleosome imaging (Figure 23, Figure 26 and Figure 27)

4. DISCUSSION

In this study, I used a combined strategy using FCS, Metropolis Monte Carlo computer simulations, and single nucleosome imaging to investigate the dynamic aspects of chromatin in living mammalian cells. The obtained restricted movement model implies that nucleosomes can move freely and rapidly in certain restricted areas, which is consistent with the fact that each nucleosome is connected by linker DNA in a manner similar to “a dog on a leash.” This restricted local movement of the nucleosomes facilitates the movement of protein molecules in chromatin, and chromatin accessibility, especially in a condensed chromatin environment, such as interphase heterochromatin or mitotic chromosomes.

In our previous paper, we proposed that interphase and mitotic chromatin are locally indistinguishable (Maeshima *et al.*, 2010b; also see Bouchet-Marquis *et al.*, 2006; Cremer T *et al.*, 2011): even in the interphase nuclei, numerous compact chromatin domains (chromatin clumps) are already present. This is in good agreement with the fact that in terms of protein diffusibility and local nucleosome dynamics, I did not detect large differences between interphase and mitotic chromatin (Figure 12 and Figure 23). This is also consistent with the finding by Bancaud *et al.* that dense heterochromatin regions are readily accessible to diffusing proteins (Bancaud *et al.*, 2009). Meanwhile, during the course of the FCS measurements, I found that EGFP mobility was severely

impaired in apoptotic chromatin that is highly condensed (Figure 31). Their D was threefold smaller than that in mitotic chromosomes, while the cytoplasm in interphase, mitotic, and apoptotic cells did not show such small D s. Thus, although both are highly condensed, the nature of the compaction state of mitotic and apoptotic chromatin seems to be distinct (Figure 31; and also see Figure 12), suggesting that the nucleosomes in “dying cells” were aggregated and their local movement diminished, different from those in living cells.

The compaction state of chromatin has been so far discussed in terms of “average pore size”: more compact chromatin shows a smaller pore size and vice versa (Gorisch *et al.*, 2005; Wachsmuth *et al.*, 2008). However, this model cannot explain why topoisomerase II α (~340 kDa in dimer) (Tavormina *et al.*, 2002) and the condensin complex (~600 kDa) (Gerlich *et al.*, 2006), which are comparable or larger than nucleosomes, show a considerable mobility inside the compact chromosomes (pore size, ~10 nm). The local dynamic property can overcome this problem: the constant local movements and rearrangements of nucleosomes allow large protein complexes to move around inside chromosomes. Since topoisomerase II α and condensin are essential for the chromosome assembly process (Losada and Hirano, 2005; Maeshima and Eltsov, 2008), this local nucleosome dynamics might also contribute to their function in the

structural maintenance of chromosomes.

Using the GFP-LacI/LacO array, which represents a large region covering 20–50 nucleosomes (Straight *et al.*, 1996; Belmont *et al.*, 1999; Heun *et al.*, 2001; Vazquez *et al.*, 2001), some groups have reported chromatin movements in living mammalian cells (Chubb *et al.*, 2002; Levi *et al.*, 2005). The reported mobility of the GFP-LacI signal is ATP-dependent and very slow at $\sim 1 \times 10^{-4} \mu\text{m}^2/\text{s}$. In addition, the mobility of DNA double strand break (DSB) sites is $1.6 \times 10^{-4} \mu\text{m}^2/\text{s}$ (Jakob *et al.*, 2009), comparable to that of the GFP-LacI signal. Meanwhile, the local nucleosome movement I identified in this study could be very rapid in a short time period: the apparent D of the nucleosomes at 0–30 ms was at least $\sim 0.025 \mu\text{m}^2/\text{s}$ (interphase) and $0.038 \mu\text{m}^2/\text{s}$ (mitotic chromosomes) (thin broken lines in Figure 24). These values are roughly 100-fold higher than the D s of GFP-LacI signals and DSB, which represent rather large chromatin fiber regions. Thus, local nucleosome movement is distinct from that observed with these large chromatin fibers. Notably, Figure 23 shows that the mean nucleosome movement within 30 ms is significantly larger than 30 nm (51 nm in the x - y plane in interphase chromatin; 59 nm in the x - y plane in mitotic chromosomes). This finding also supports our notion that almost no 30-nm chromatin fibers exist in mitotic chromosomes (Maeshima *et al.*, 2010a; Nishino *et al.*, 2012) as well as in the

majority of active interphase chromatin (Maeshima *et al.*, 2010a; Fussner *et al.*, 2011).

This study revealed the local dynamic property of chromatin in interphase and mitotic living cells. Such a property facilitates protein diffusibility and targeting in chromatin, and chromatin accessibility (Figure 15, Figure 16 and Figure 29). These aspects are essential in many biological processes. For example, upon scanning genome information, the dynamic local movement of nucleosomes can facilitate targeting of transcription complexes by exposing target DNA sequences more often than would static folding structures. This advantage would also be true for many other biological processes such as DNA repair, replication, and recombination (Figure 32).

5. FIGURES AND FIGURE

LEGENDS

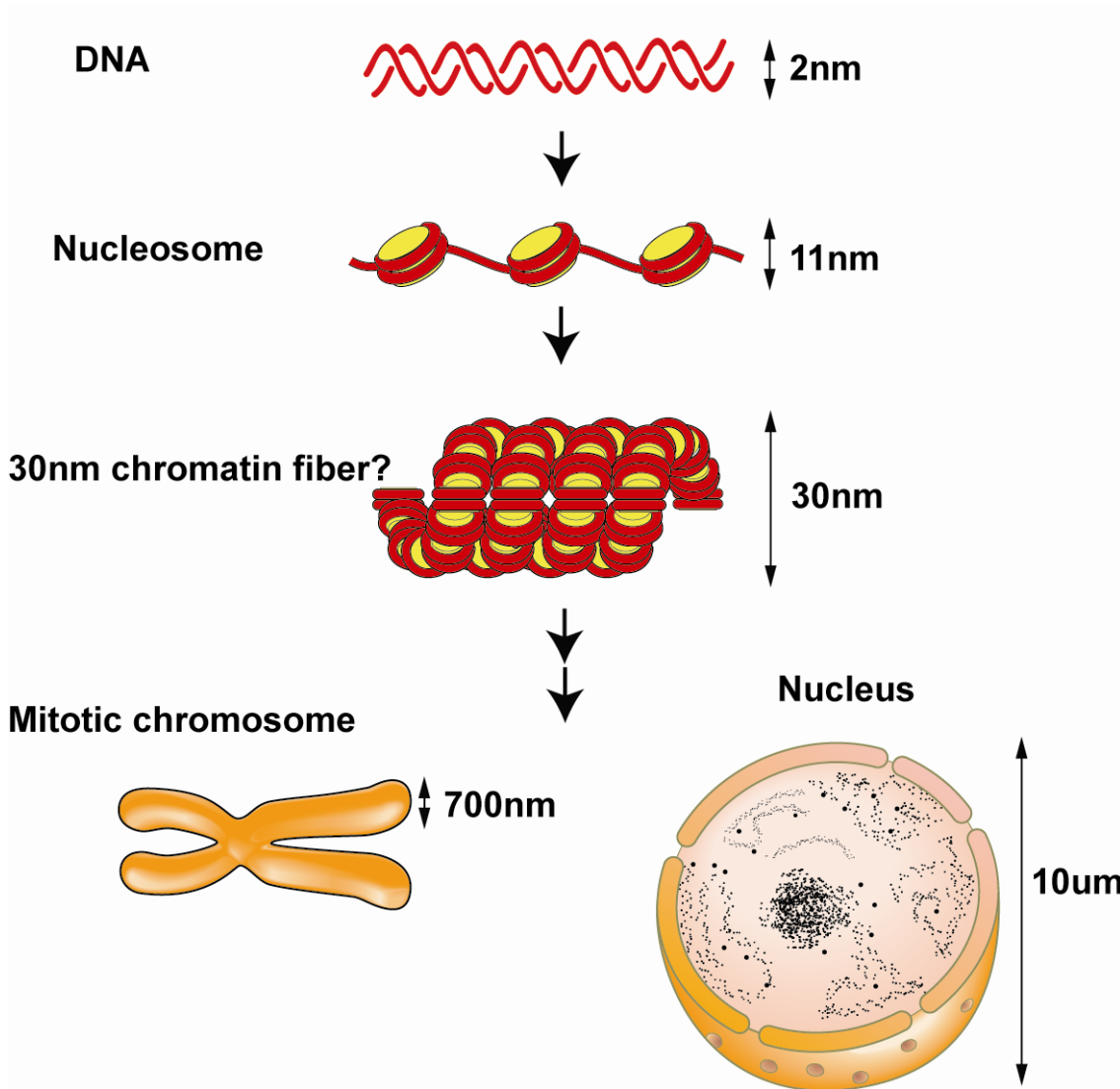


Figure 1

Figure 1. Chromatin structure

A long DNA with a diameter of 2-nm is wrapped around a core histone octomer that consist of H2A, H2B, H3 and H4 histones and forms a ‘nucleosome’ with a diameter of 11nm. The nucleosome has long been assumed to be folded into 30-nm chromatin fibers before the higher order organization of mitotic chromosomes or interphase nuclei

occurs.

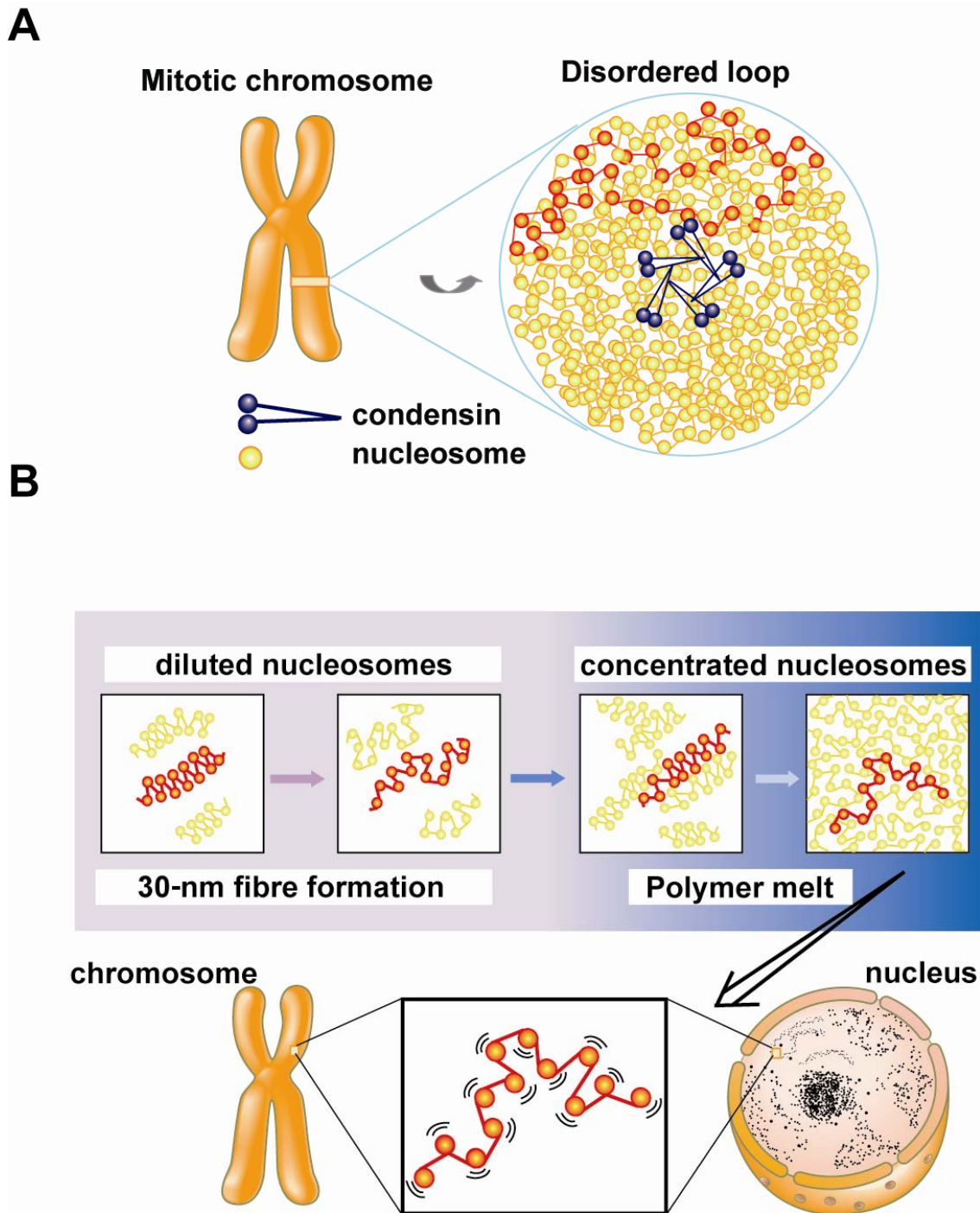


Figure 2

Figure 2. Novel chromatin structure model based on the polymer melt hypothesis

(A) Chromosomes consist of irregularly folded nucleosome fibers globally around the

chromosome centre.

(B) Under diluted condition, the flexible nucleosome fibers can take intra-fiber nucleosome associations, forming the 30-nm chromatin fibers. An increase in nucleosome concentration results in inter-fiber nucleosomal contacts, which interfere with the intra-fiber associations. The concept of polymer melt implies dynamic polymer chains, that is, nucleosome fibers may be moving and rearranging constantly at local level.

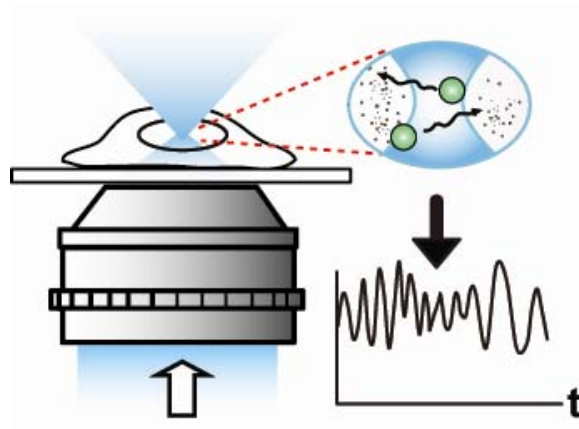


Figure 3

Figure 3. Schematic diagram of FCS measurement

FCS detects in-out motion of EGFP molecules (green balls) at a ~ 0.1 femto-liter volume (white region in the blue cylinder) as fluctuations in fluorescence intensity (shown as a graph).

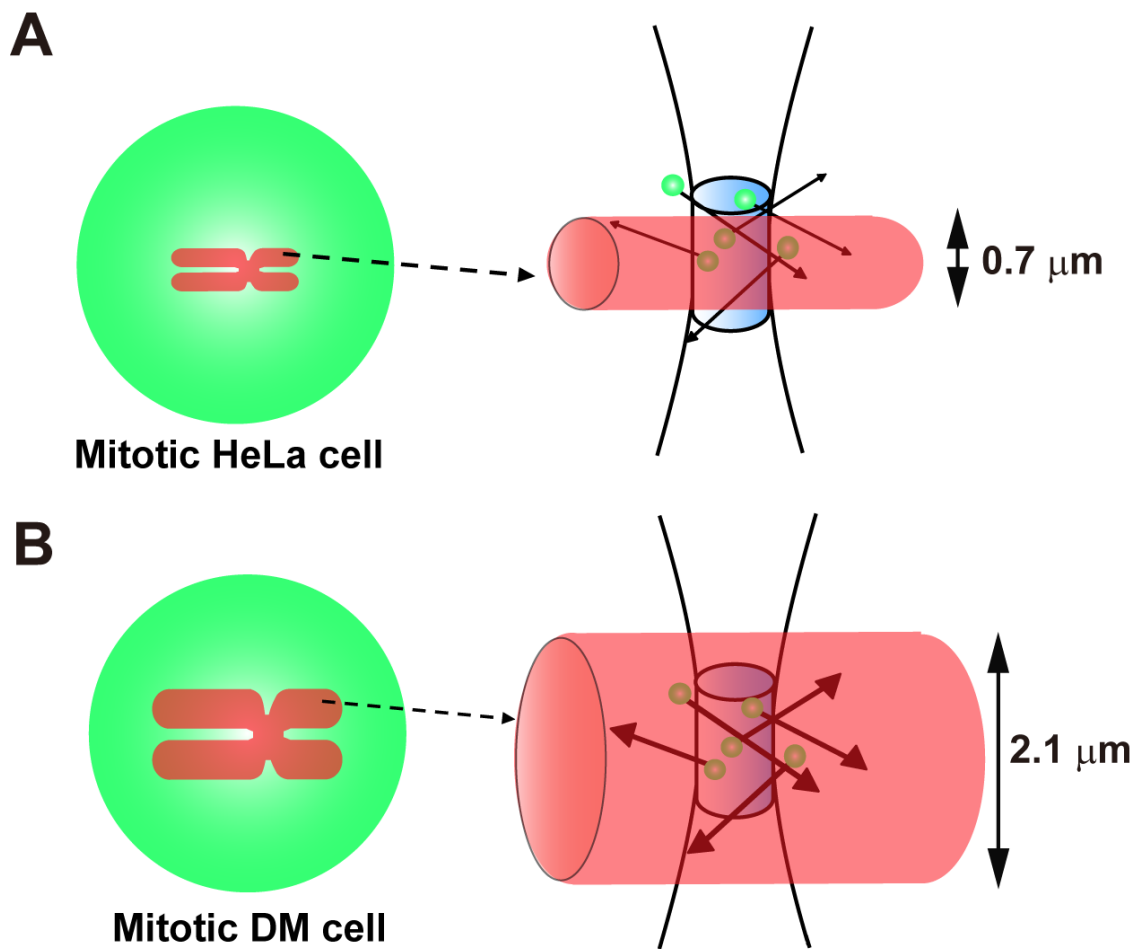


Figure 4

Figure 4. The cell line suitable for inspecting the chromosome environment

(A) The detection volume (1-2 μm) is much larger than human chromosomes (0.7 μm) and contains the cytoplasm when FCS measurement. On the other hand, the giant DM chromosome (2.1 μm) is larger than the detection volume (B).

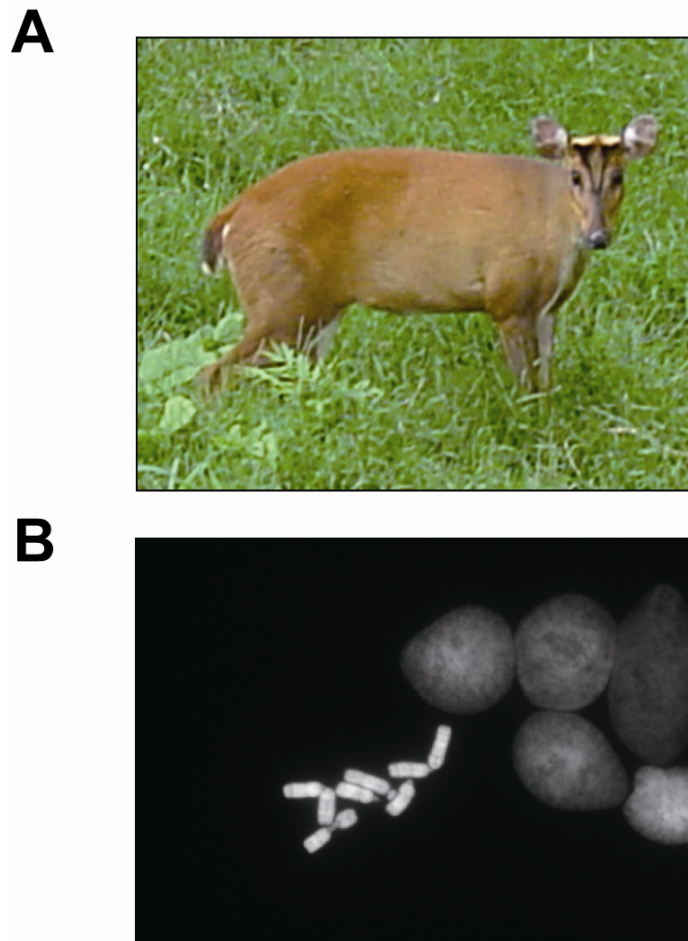


Figure 5

Figure 5. Indian Muntjac and Indian Muntjac cell (DM cell) chromosomes

(A) Indian muntjac is the most numerous muntjac deer species. They are widespread throughout Southern Asia (a photo from Wikipedia Commons).

(B) The number of their chromosome is 6 or 7 (female: $2n = 6$ male: $2n = 7$). A similar Muntjac (Chinese Muntjac) has a number of 46 chromosomes.

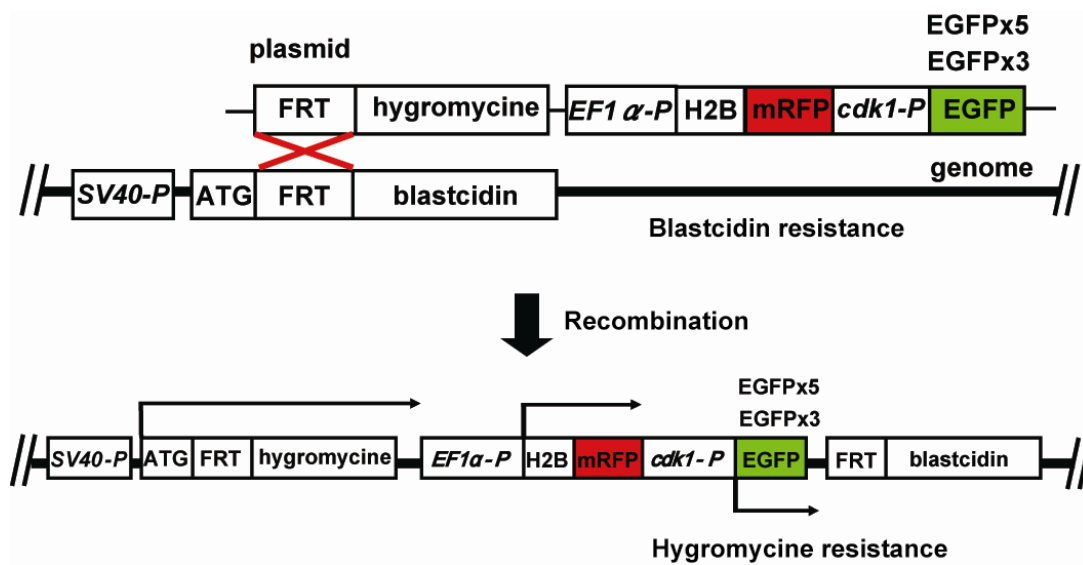


Figure 6

Figure 6. Schematic representation of introduction of the constructs into the Indian Muntjac (DM Cell) genome

The construct was inserted into the FRT site that had been introduced to the DM genome in advance via F1p recombinase-mediated DNA recombination. With the correct recombination, DM cells became hygromycin-resistant and blastcidin-sensitive.

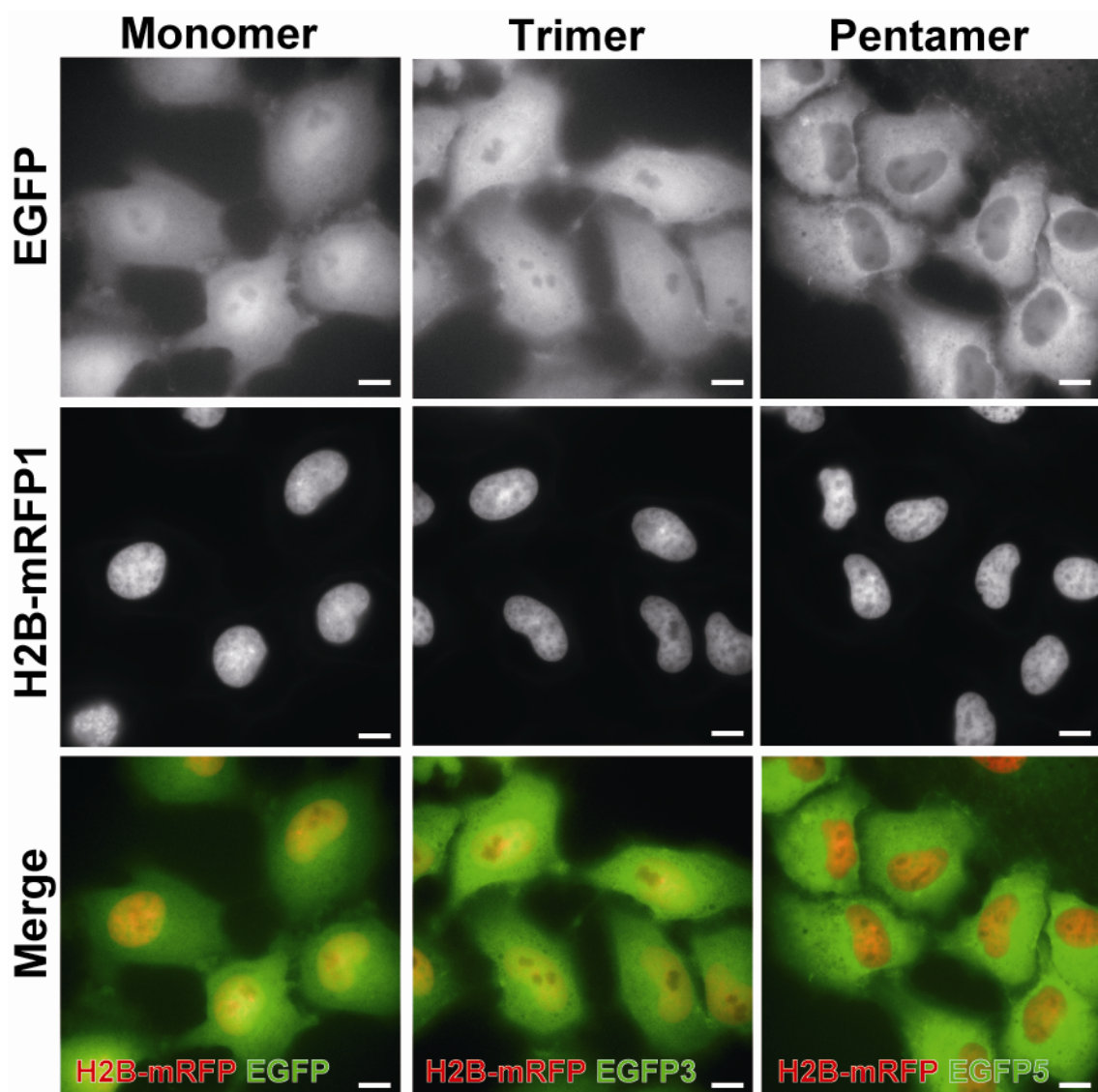


Figure 7

Figure 7. DM cell lines expressing EGFP-monomer, trimer, and pentamer

EGFP signal (first row); H2B-mRFP1 (second row); merged images (third row).

Note that EGFP-monomer and trimer were quite uniformly distributed in the cytoplasm and nuclei. The pentamer signal in the nuclei was also uniform, although its signal was weaker than that in the cytoplasm, probably because the pentamers cannot pass through the nuclear pores. Bar shows 10 μm .

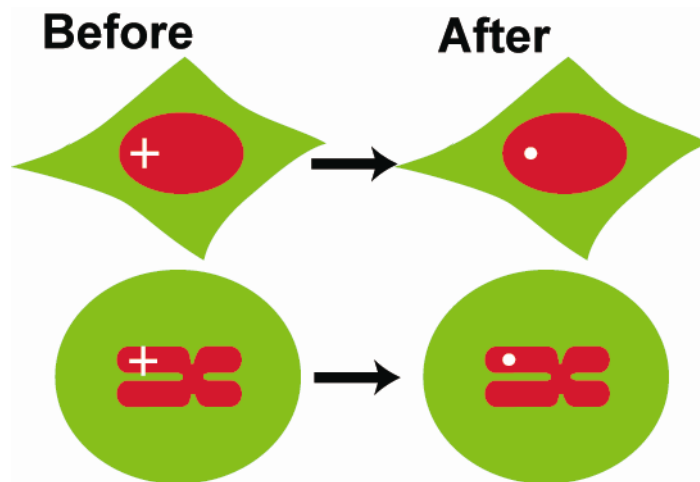


Figure 8

Figure 8. Photobleaching of H2B-mRFP1 after FCS measurement

The chromatin regions (red) are photobleached out after FCS and the actual measured regions (white) could be identified in the interphase chromatin (upper) and mitotic chromosomes (lower) by z-stack imaging by confocal microscopy (LSM510).

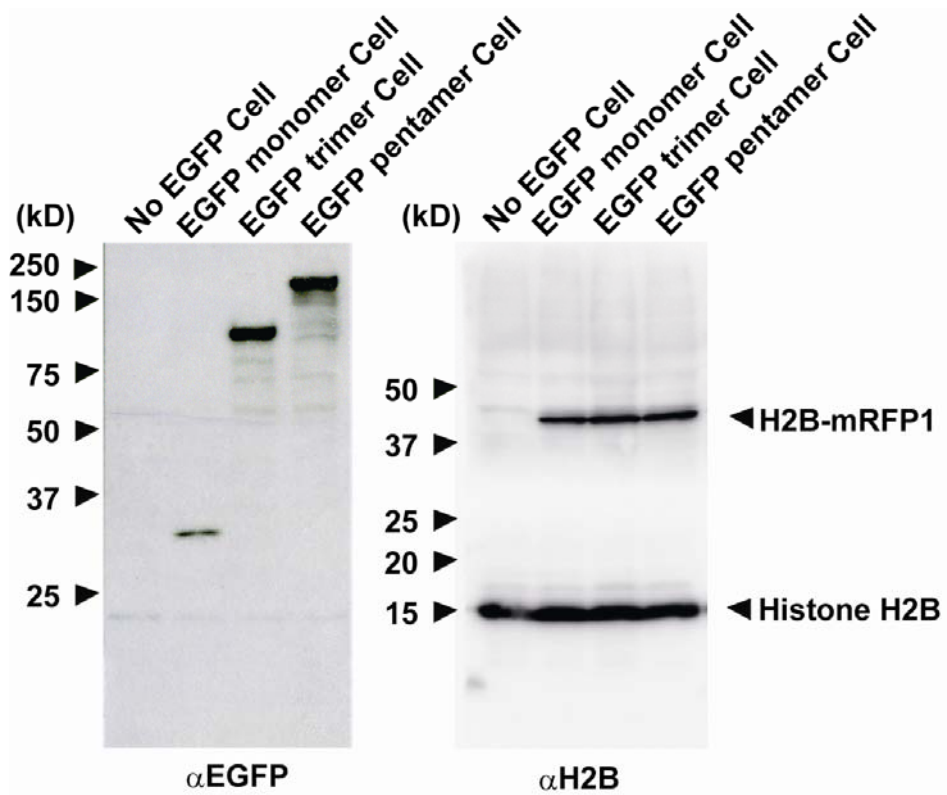


Figure 9

Figure 9. Verification of proper expression of EGFP-monomer, trimer, and pentamer (Left) and H2B-mRFP1 (Right)

Total cell lysates from normal DM cells and DM cell lines expressing the tandem EGFPs (left) and H2B-mRFP1 (right) were analyzed by Western blotting using antibodies against H2B, mRFP1, and EGFP.

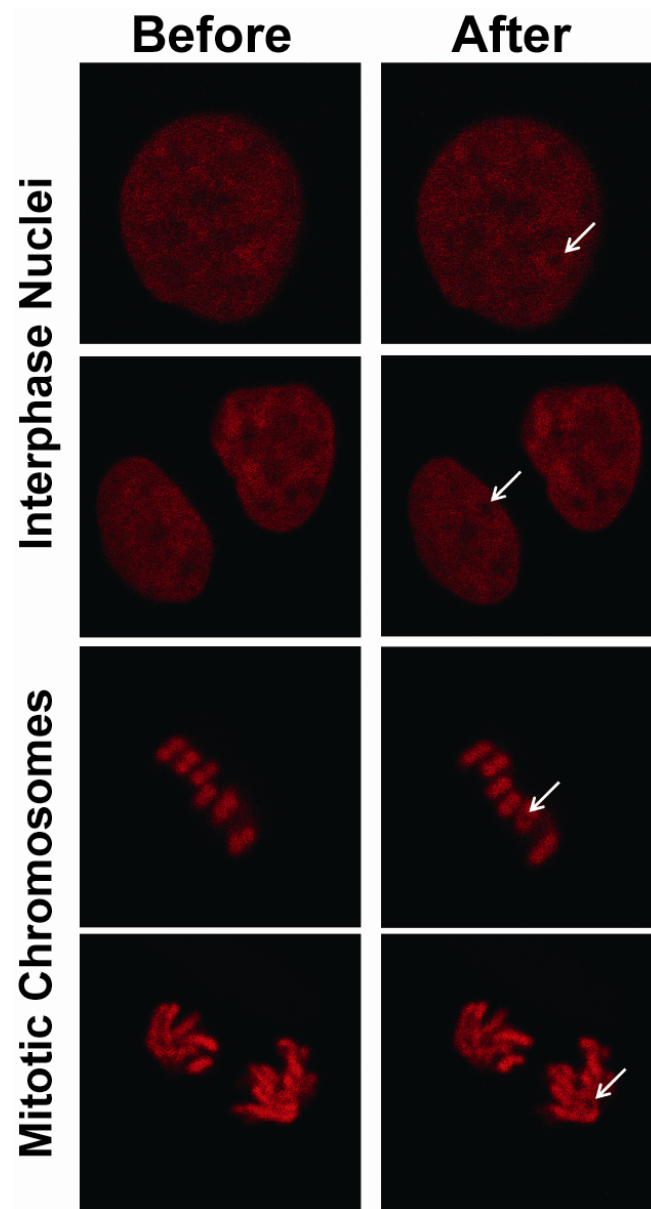


Figure 10

Figure 10. Photobleaching of H2B-mRFP1 after FCS measurement in living cells

Chromatin regions (red) are photobleached before (left column) and after (right column)

FCS; the actual measured regions (arrows) were verified in interphase chromatin

(upper) and mitotic chromosomes (lower). Note that these images were obtained using a

high-power laser to visualize the bleached sites.

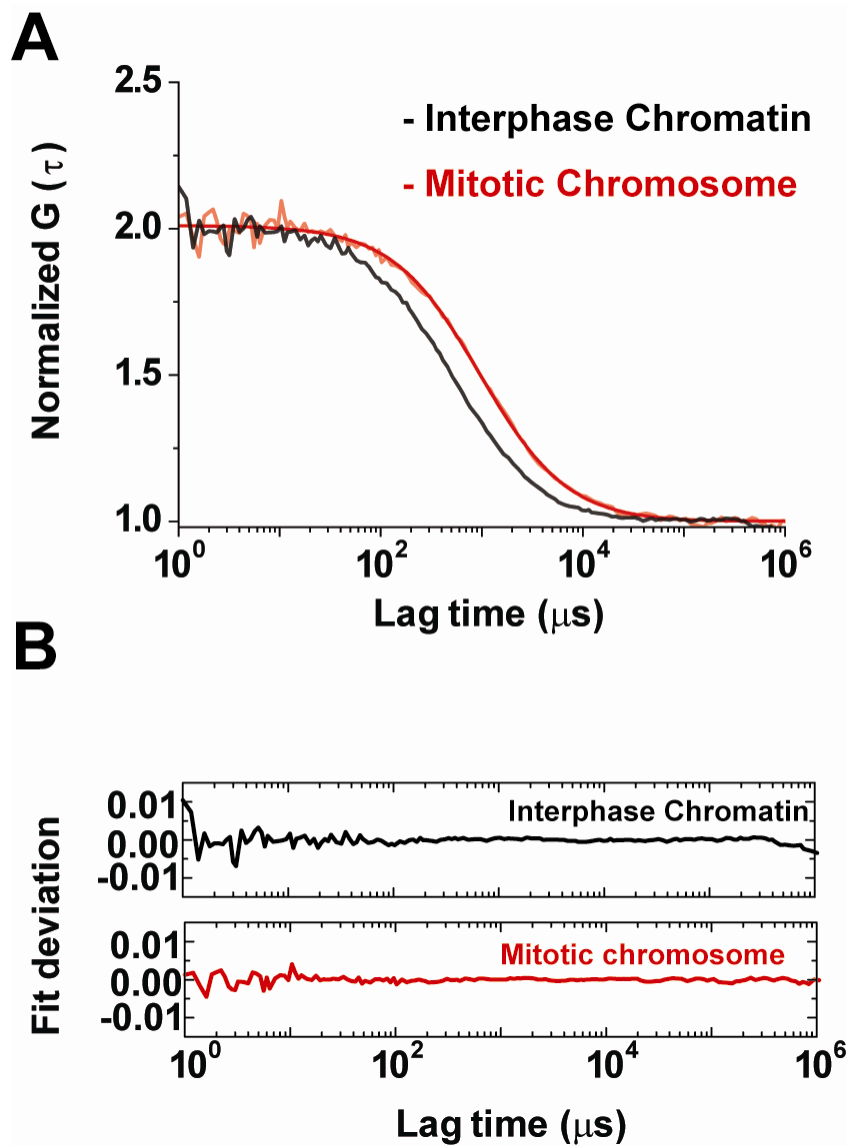


Figure 11

Figure 11. Normalized fluorescence autocorrelation functions (FAFs) of the EGFP-trimer in living interphase (Black Line) and mitotic (Red Line) cells

(A) The fitting was performed using a one-component model. (B) Deviation of the fit throughout the lag time, demonstrating that the FAFs were well fit by the one-component model.

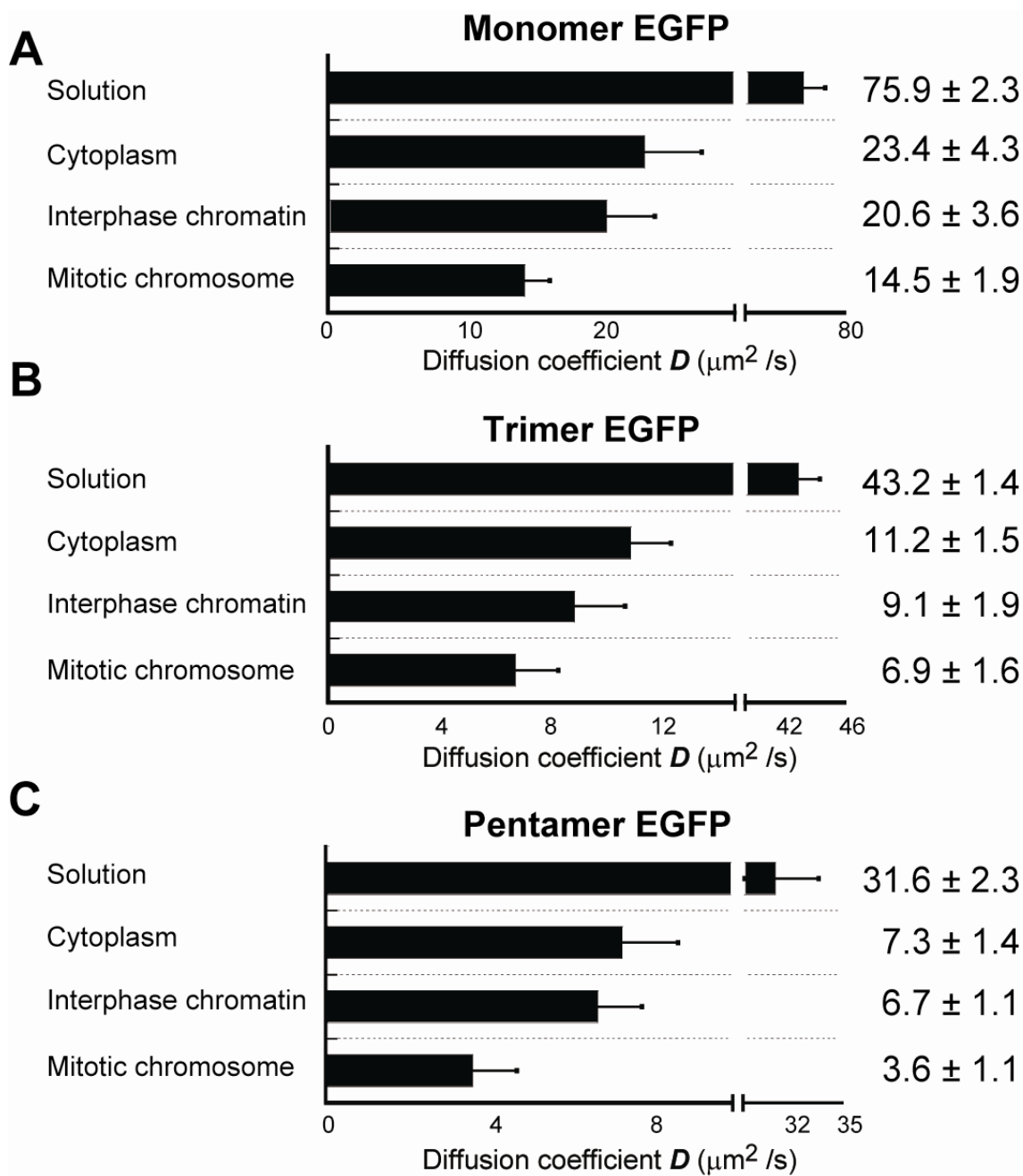


Figure 12

Figure 12. Mean values of diffusion coefficients (D s)

D s of EGF-Monomer (A), Trimer (B), and Pentamer (C) in Solution (First Row, Pack et al., 2006) and Cytoplasm (Second Row), Interphase Chromatin (Third Row), and Mitotic Chromosomes (Fourth Row)

For details of the D calculation, see Experimental Procedures. The mean value and standard deviation (SD) are shown on the right ($n = 5$).

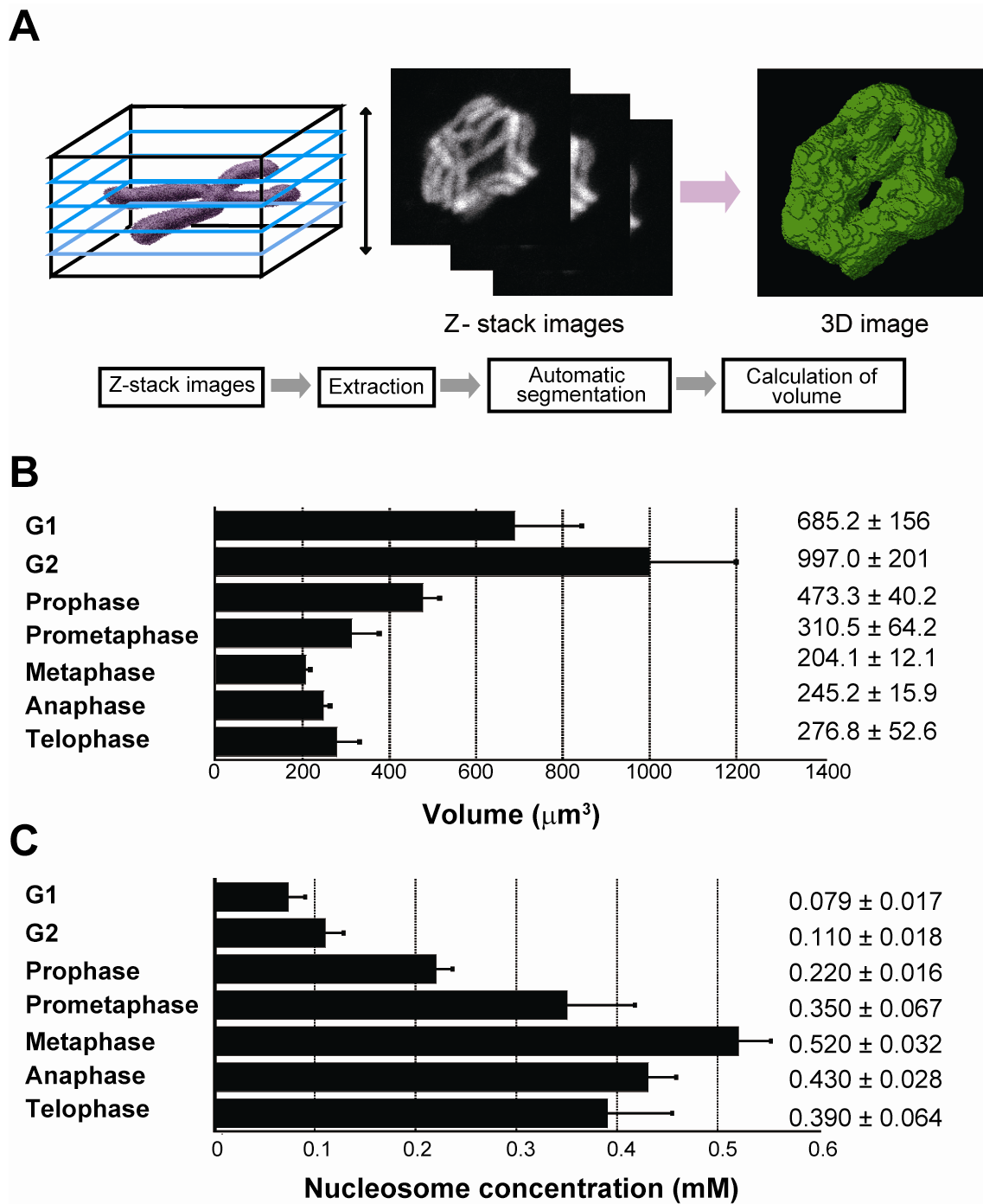


Figure 13

Figure 13. Measurements of nucleosome concentrations in interphase nuclei and mitotic chromosomes

(A) Chromatin regions were extracted and segmented from the 3D-image stacks using a

novel extraction and segmentation procedure (left two images; for details, see Experimental Procedures), and the nuclear and chromosome volumes were calculated from the segmented areas. Note that since the chromosome clusters, especially in anaphase, have a complicated shape, chromosome volumes may have been underestimated. The obtained volumes (**B**) and concentrations (**C**) are shown as bar graphs (left), and their mean values and SD are shown on the right ($n = 4$).

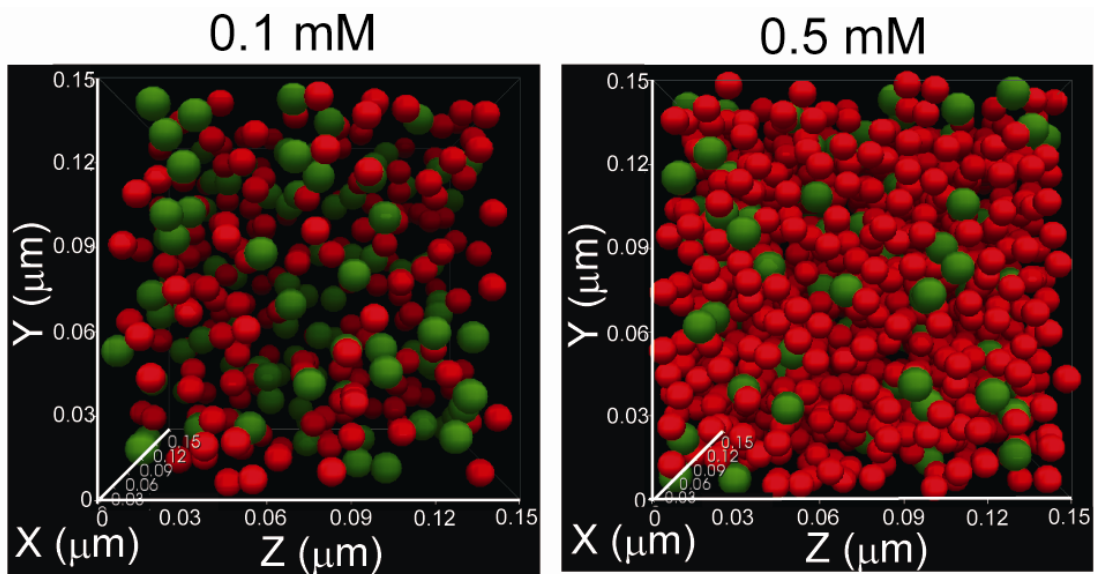


Figure 14

Figure 14. Reconstructions of the living chromatin environment by Metropolis Monte Carlo Computer Simulations

The nucleosome is represented as a spherical hardbody (red ball) with diameter of ~ 10 nm and fixed in a restricted space at a concentration of 0.1 mM (left image) and 0.5 mM (right image, corresponding to mitotic chromatin or interphase heterochromatin), randomly but in a manner to avoid any overlap. The EGFP-pentamer molecule is represented as a spherical ball (green ball) with a 13 nm diameter (see Experimental Procedures).

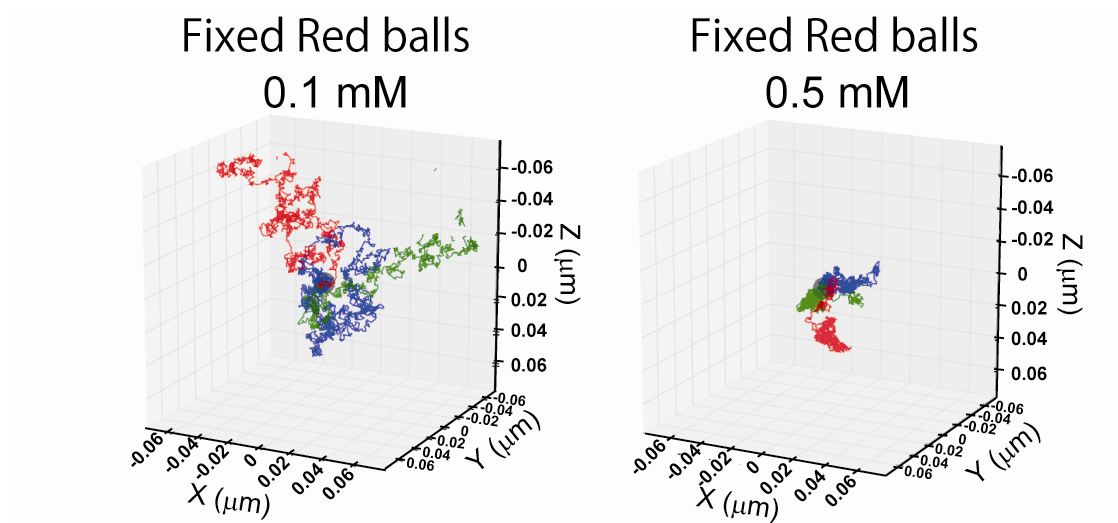


Figure 15

Figure 15. The trajectories of the diffusing green balls (EGFP-pentamer molecules) in fixed red ball environments

The green balls were put in random motion avoiding the red balls at the obtained D ($7.0 \text{ mm}^2/\text{s}$).

With 0.1 mM fixed red balls, the green balls moved around freely (left image). However, with 0.5 mM fixed red balls, they could not move far from their starting points (right image). The three different temporal trajectories of green balls for 0.2 ms are indicated by blue, green, and red.

Fluctuated Red balls 0.5 mM

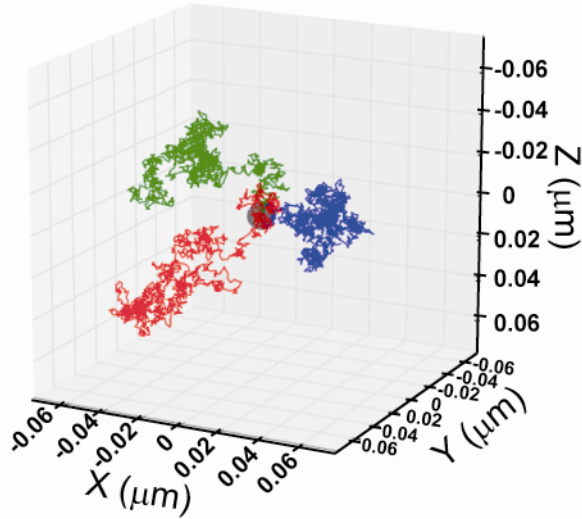


Figure 16

Figure 16. The trajectories of the diffusing green balls in fluctuated red ball environment

In the environment with fluctuation of 0.5 mM red balls, the green balls could move around freely, in contrast to the case of fixed red balls (right in Figure 15). Each red ball behaved like “a dog on a leash.” The lead length was 20 nm.

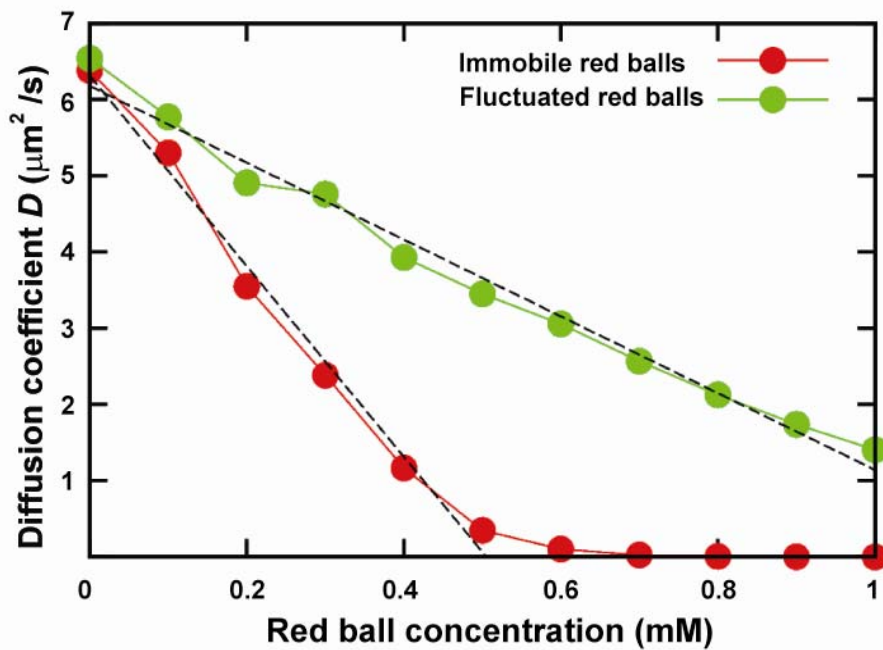


Figure 17

Figure 17. Terminal diffusion coefficients (D s) of green balls with various nucleosome concentrations, which were fixed (Red) or fluctuated (Green)

Note that 0.5 mM fixed red balls did not allow the green balls to move around freely, consistent with Figure 15. The “dog leash” [maximum nucleosome displacement (movement)] length was 20 nm.

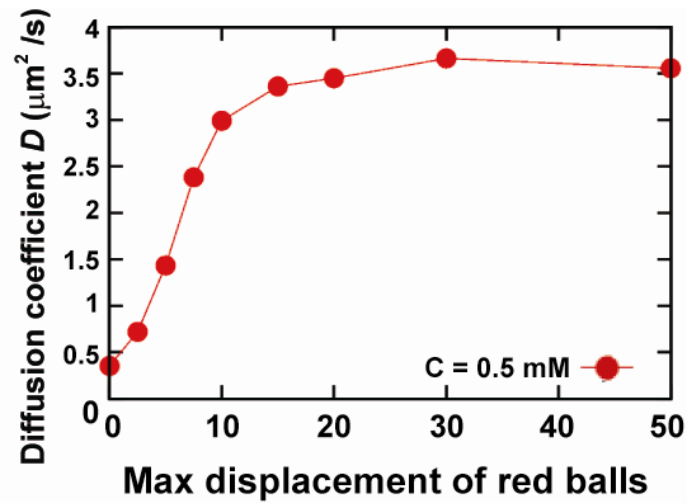


Figure 18

Figure 18. Terminal D s of the green balls with 0.5 mM red balls and various “dog leash” lengths (maximum displacement of nucleosomes)

Note that a maximum displacement (movement) of red balls of 20 nm allowed green balls to diffuse quite freely.

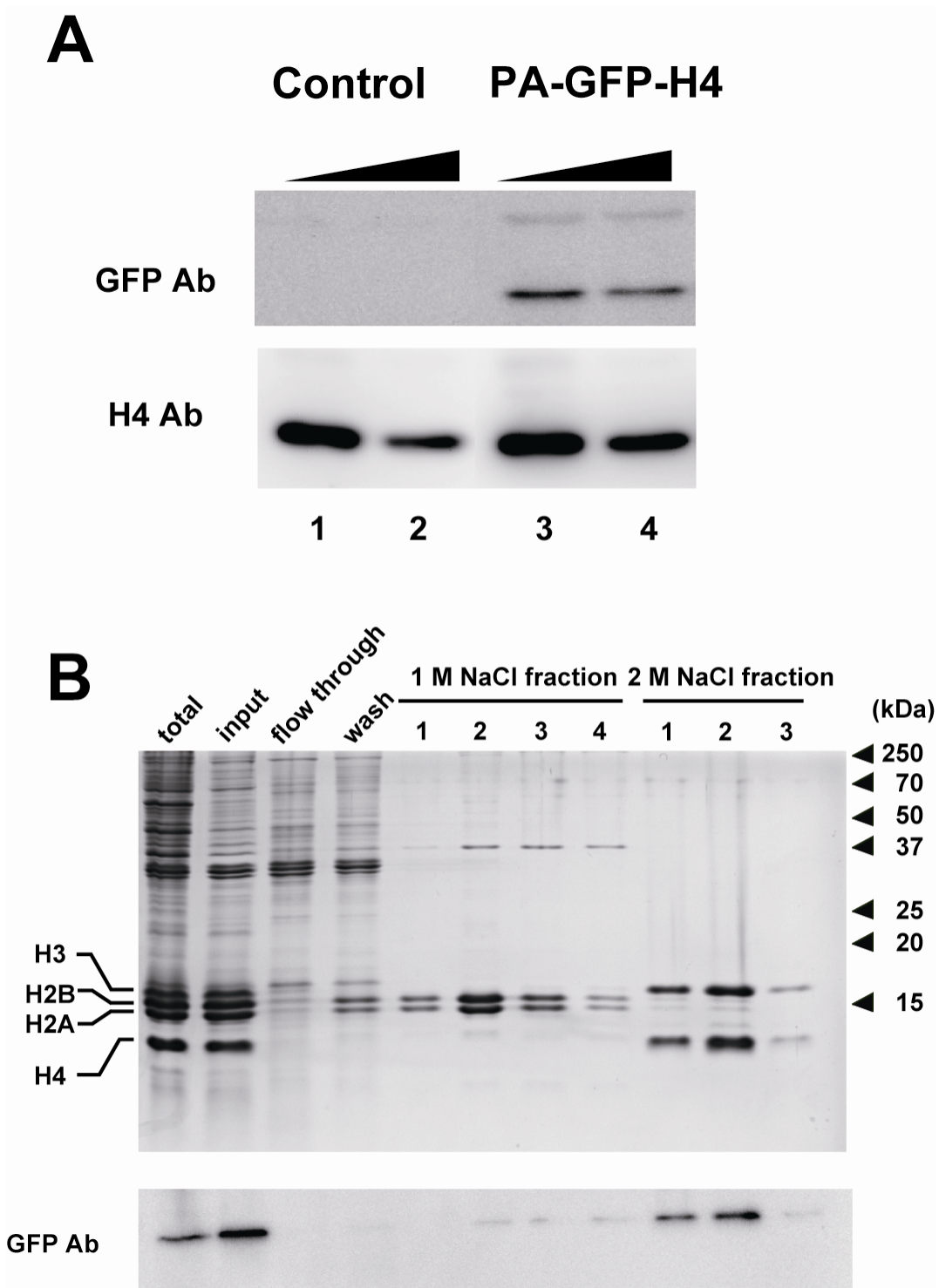


Figure 19

Figure 19. Structural integrity of nucleosomes containing PA-GFP-H4

(A) Verification of proper expression of PA-GFP-H4. Total cell lysates from control DM cells (left) and those expressing PA-GFP-H4 (right) were analyzed by Western blotting with antibodies against EGFP (upper) and histone H4 (lower). **(B)** Salt extraction of PA-GFP-H4 from chromatin in the DM cells. Chromatin fractions were prepared from the nuclei (total) of the DM cells expressing PA-GFP-H4 and loaded onto HTP (input and flow-through). After washing (wash), histone fractions were eluted in a stepwise manner with 1 M NaCl (fractions 1–4) and 2 M NaCl (fractions 1–3). Eluates were separated on SDS-PAGE gels and either stained with Coomassie Brilliant Blue (upper) or blotted using an antibody against GFP (lower). Note that the elution profile of PA-GFP-H4 was similar to that of endogenous H4, verifying the structural integrity of the nucleosomes containing PA-GFP-H4. Since anti-H4 antibody (2000-fold dilution, Upstate 07-108) readily detected histone H4 but not PA-GFP-H4 (Hihara, unpublished data) in the cell lysates, I estimated that the number of PA-GFP-H4 molecules in the nucleosomes was less than 5% of endogenous H4, suggesting that the incorporation probability of two PA-GFP-H4 molecules in a single nucleosome was less than 2.5×10^{-3} .

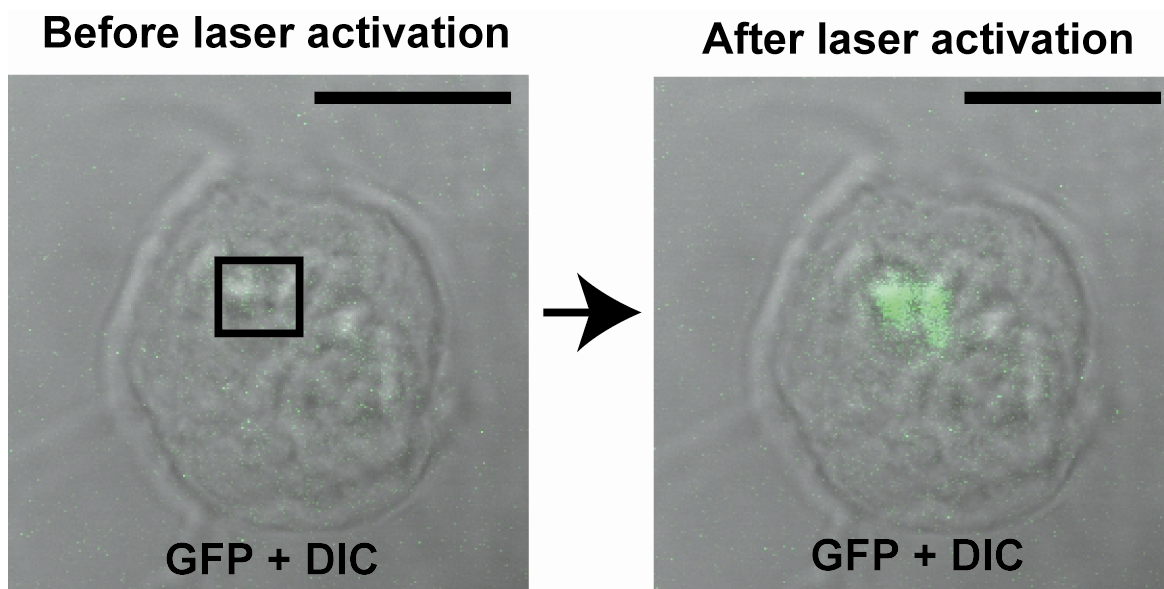


Figure 20

Figure 20. Photoactivation of PA-GFP-H4 in the DM Cells

Before photoactivation, no fluorescence signal was detected (left). After stimulation with a 405-nm laser to the black square region, the GFP signal appeared (right image), verifying the functionality of PA-GFP. Bar shows 10 μm .

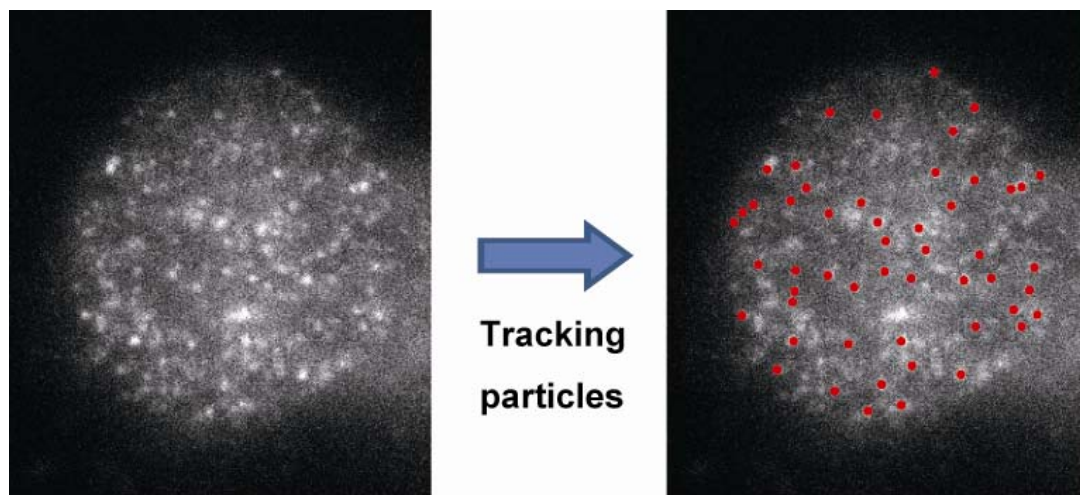


Figure 21

Figure 21. Nuclear image of DM cells expressing PA-GFP-H4

The bright particles show single nucleosomes under the HILO microscopy system (for details, see Experimental Procedures) because of the clear single-step photobleaching profile of PA-GFP-H4 dots (Figure 22).

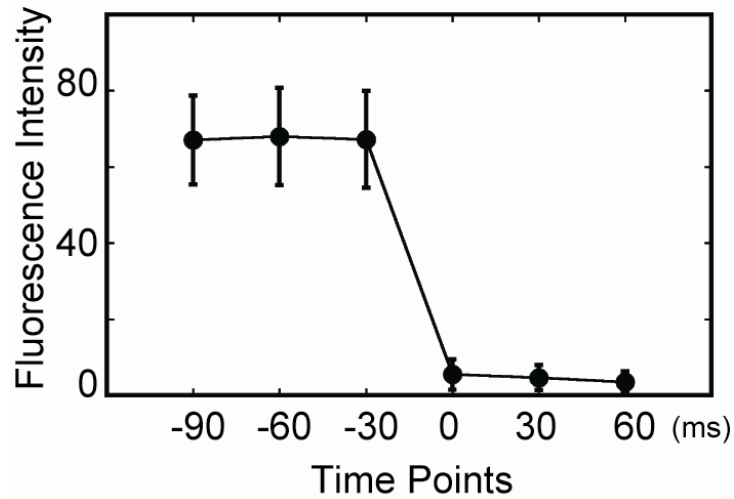


Figure 22

Figure 22. Single-step photobleaching of PA-GFP-H4 dots

The vertical axis is the fluorescence intensity of each tracked PA-GFP-H4 dot. The horizontal axis is the tracking time series (photobleaching point was set as time 0; $n = 100$). Because of the clear single-step photobleaching profile of PA-GFP-H4 dots, each dot in Figure 21 shows a single PA-GFP-H4 molecule in a single nucleosome.

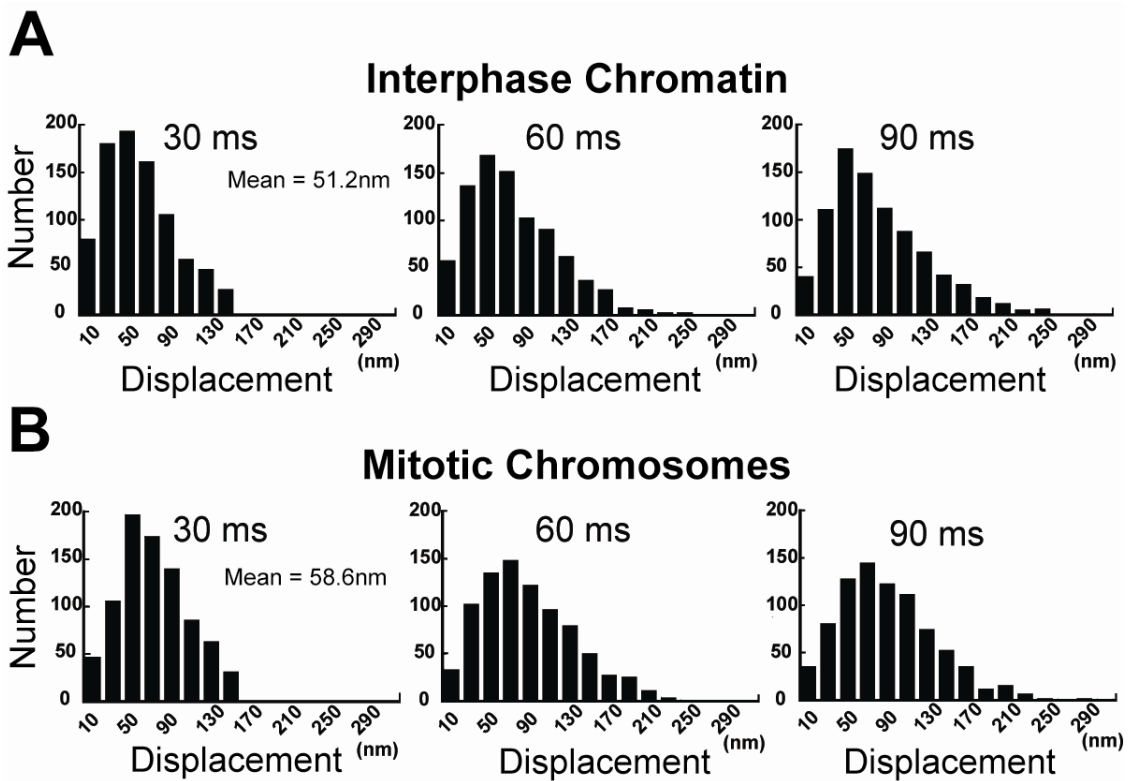


Figure 23

Figure 23. Displacement (movement) distributions of single nucleosomes

Interphase chromatin (B) ($n = 8$) and mitotic chromosomes (C) ($n = 12$) for 30 (left), 60 (center), and 90 (right) ms.

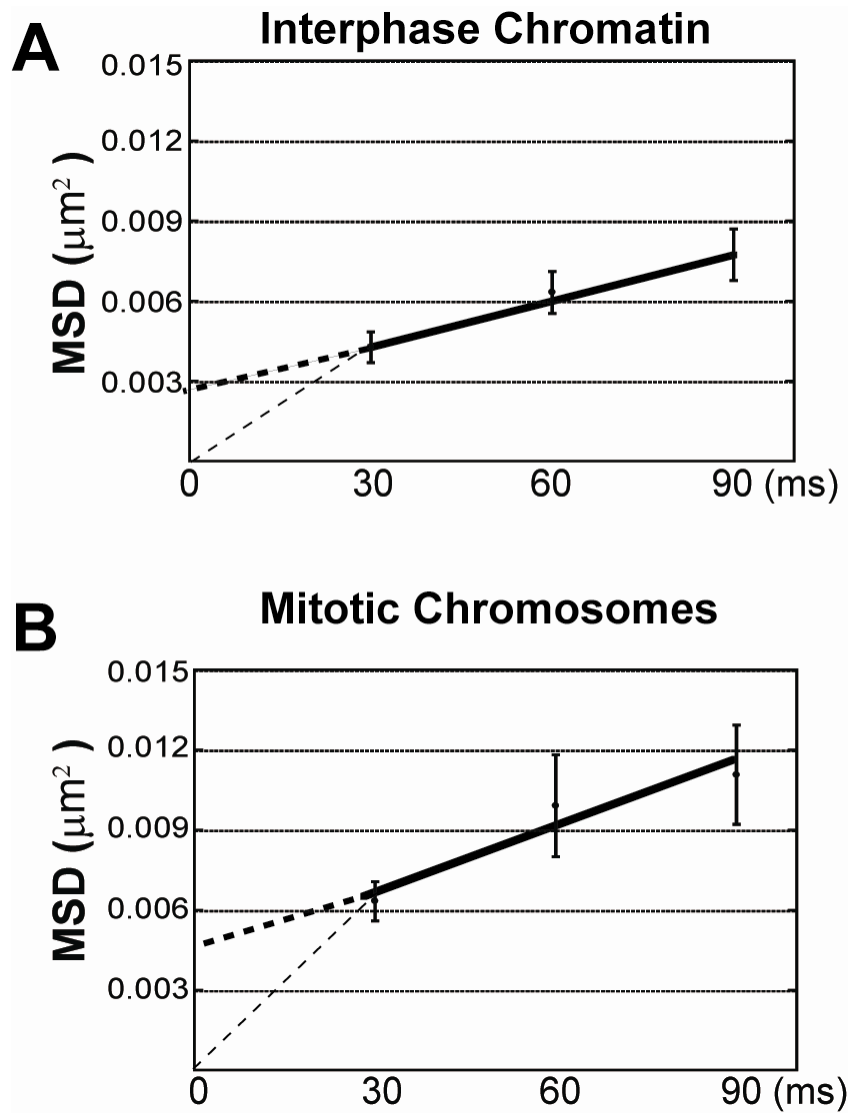


Figure 24

Figure 24. Plots of the mean square displacements (MSDs) of single nucleosomes for 30, 60, and 90 ms in interphase chromatin (A) and mitotic chromosomes (B)

The cross-linked nucleosomes in glutaraldehyde-fixed DM cells were used as a background. The plots were fitted with a linear approximation, which does not pass through the origin (thick broken lines), suggesting that the nucleosome movement

support a restricted diffusion model. The apparent D s of the nucleosomes at 0–30 ms were at least $\sim 0.025 \mu\text{m}^2/\text{s}$ (**A**, thin broken line) and $0.038 \mu\text{m}^2/\text{s}$ (**B**, thin broken line).

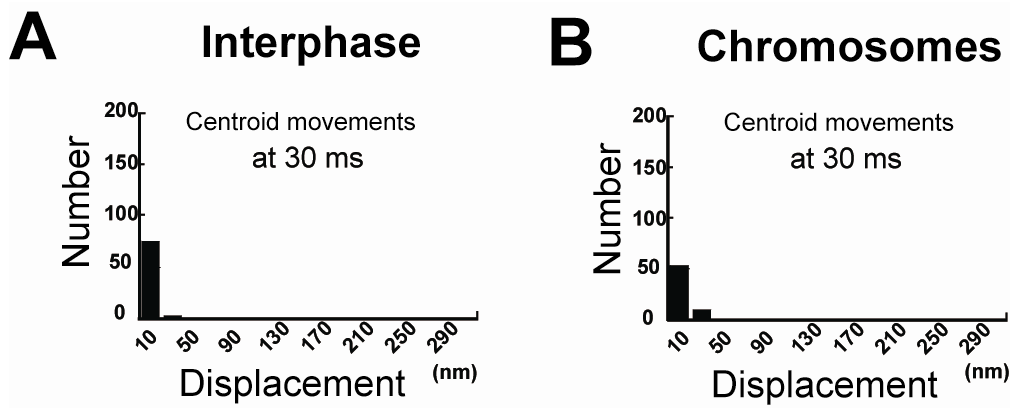


Figure 25

Figure 25. Centroid movements of a number of observed nucleosomes

Note that the centroid movements are much smaller than those in (A) and (B), suggesting that the detected nucleosome movement was not derived from the global motion of nuclei or chromosomes.

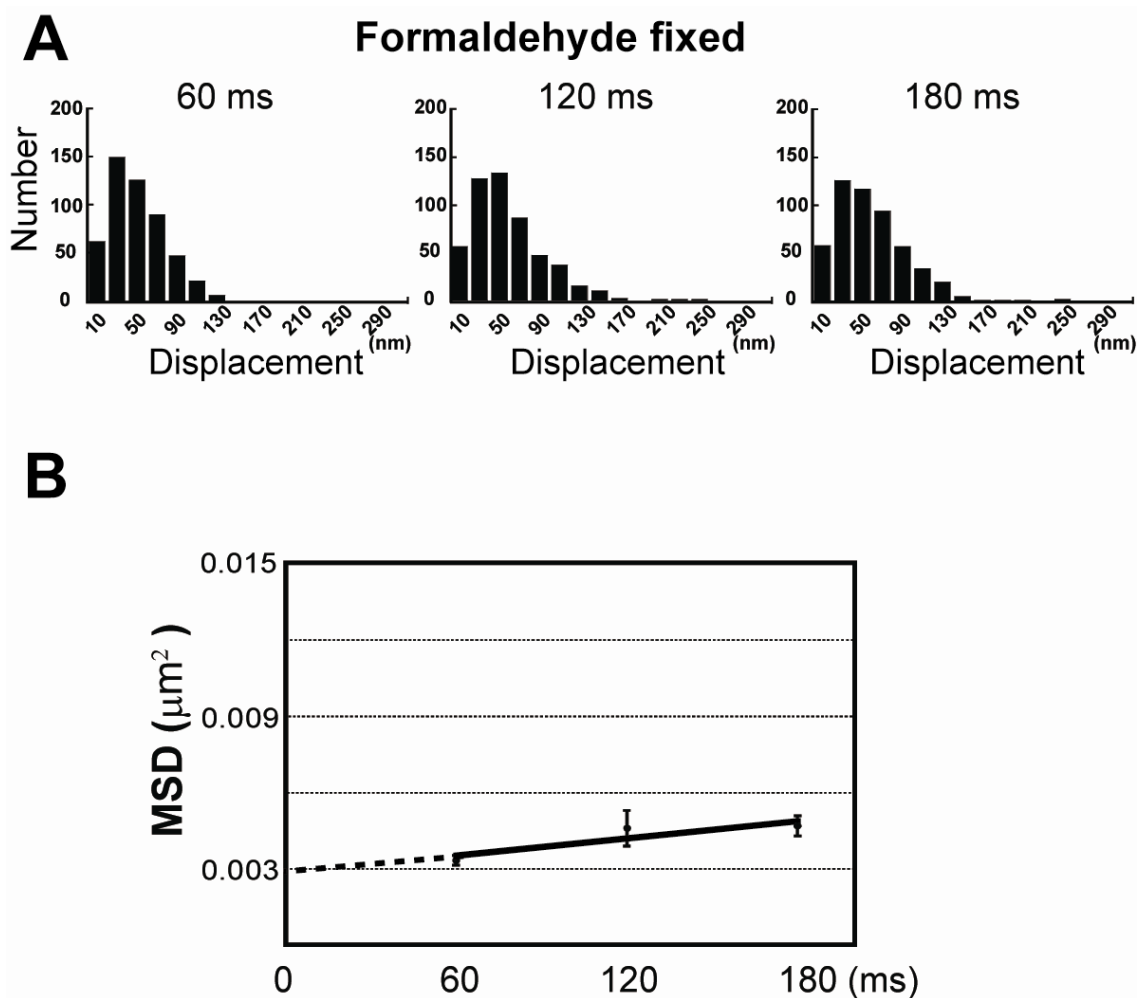


Figure 26

Figure 26. Single nucleosome movement in formaldehyde-fixed cells

(A) Displacement distributions of single nucleosomes for 60 (left), 120 (center), and 180 (right) ms. Note that formaldehyde-fixed cells still showed considerable nucleosome mobility, much more than that of glutaraldehyde-fixed cells (Figure 27).

(B) Plots of the mean square displacement (MSD) of single nucleosomes for 60, 120, and 180 ms ($n = 6$). Plots were fitted with a linear approximation.

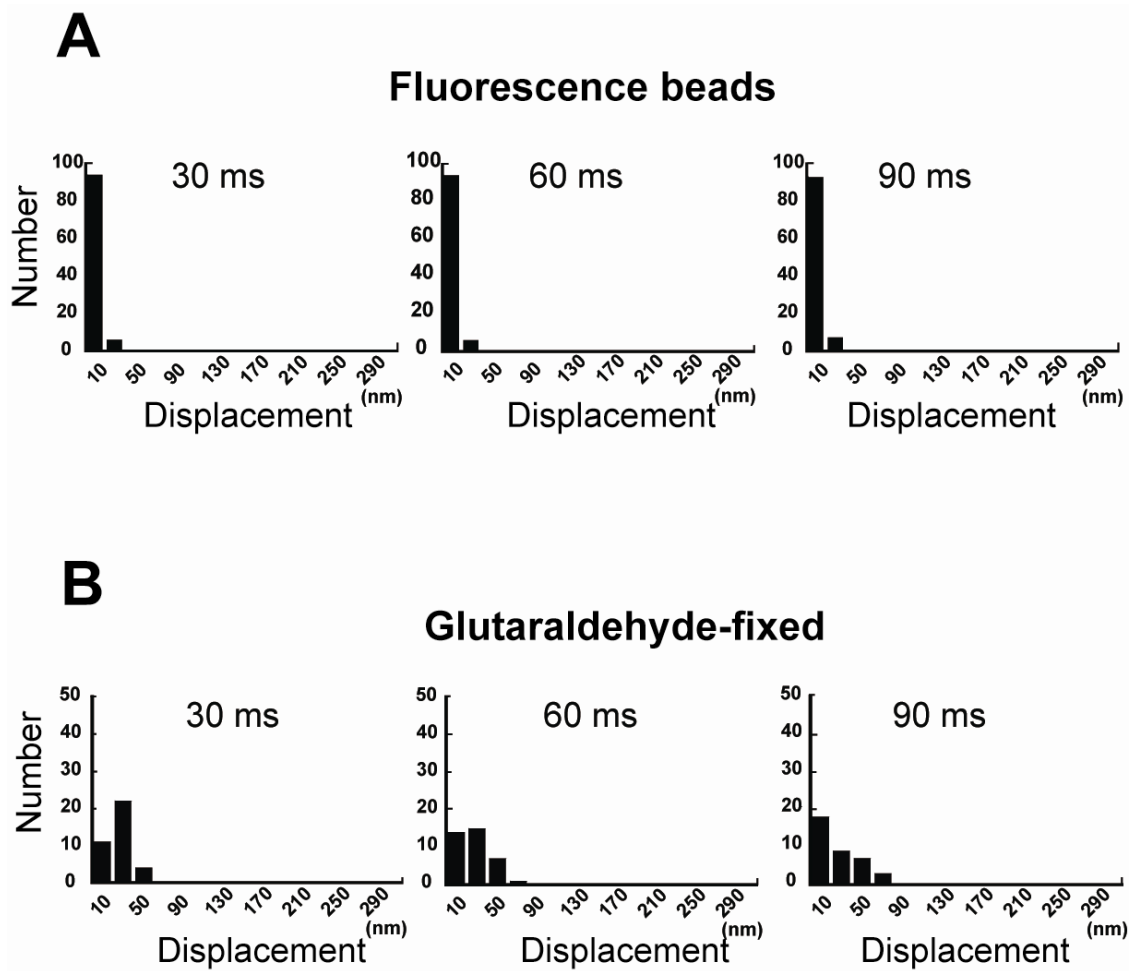


Figure 27

Figure 27. Movement of single fluorescence beads (A) ($n = 100$) and cross-linked nucleosomes in glutaraldehyde-fixed cells (B) ($n = 8$)

Displacement distributions of single fluorescence beads on a glass surface (A) and cross-linked nucleosomes in glutaraldehyde-fixed DM cells (B) for 30 (left), 60 (center), and 90 (right) ms. Note that their displacements were significantly lower than those in living cells (Figures 23).

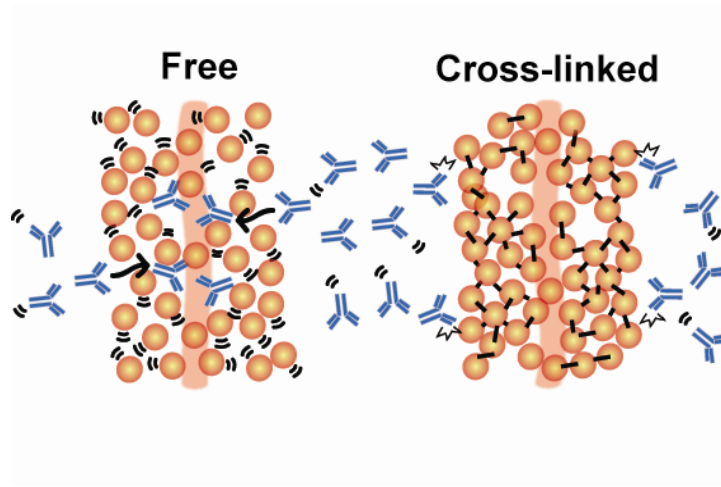


Figure 28

Figure 28. Schematic representation of the experiment

Protein accessibility and targeting to the chromatin was examined by immunostaining with anti-CAP-H2 monoclonal antibody (a condensin II component).

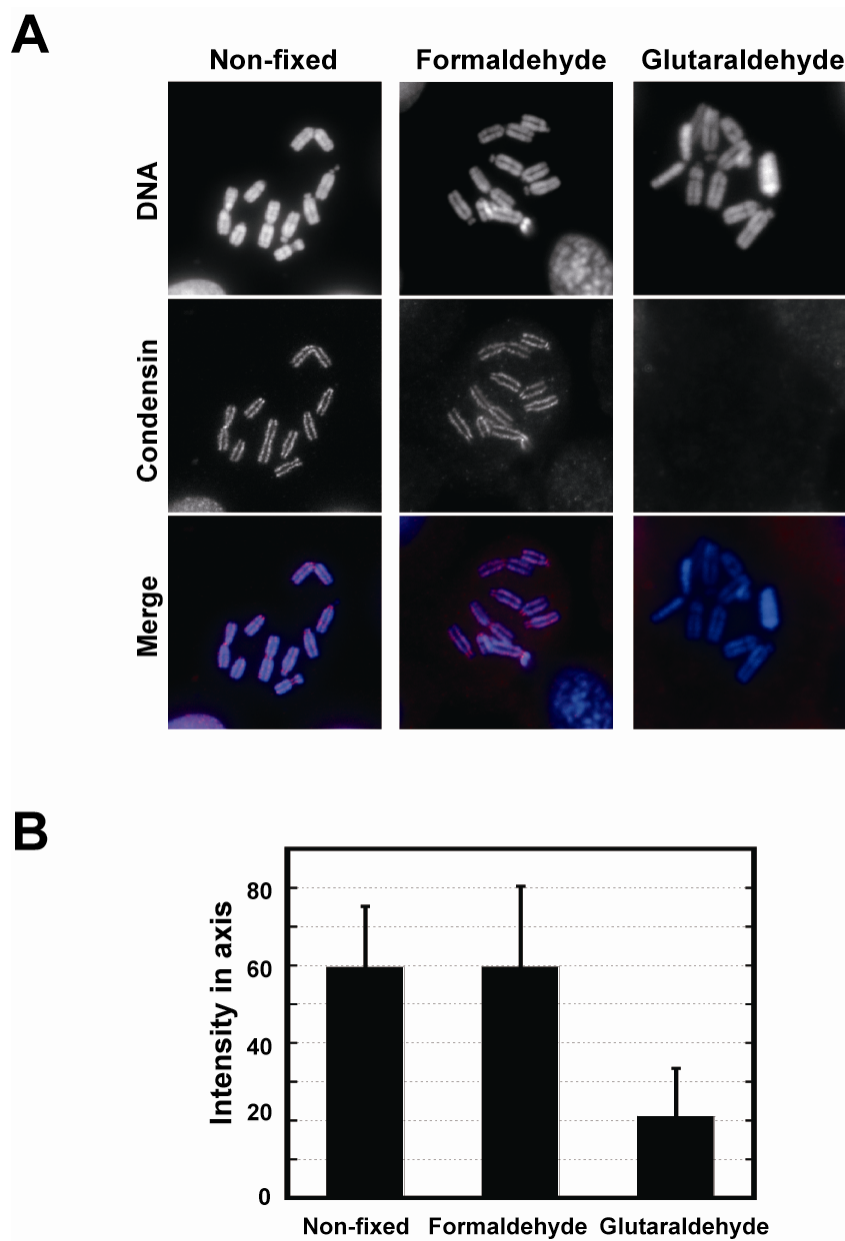


Figure 29

Figure 29. Tight cross-linking of nucleosomes blocks antibody accessibility and targeting

(A) Signals were detected in non- and formaldehyde-fixed chromosomes (left and center columns), but not in the glutaraldehyde-fixed chromosomes (right column). Note that the size of antibodies is ~15 nm (~150 kDa). (B) Intensities of axial signals were

plotted ($n = 104$). The intensities of glutaraldehyde-fixed chromosomes were significantly less than those of the others. Mitotic chromatin in formaldehyde-fixed cells and non-fixed cells had similar accessibility to diffusing proteins, although glutaraldehyde-fixed cells did not.

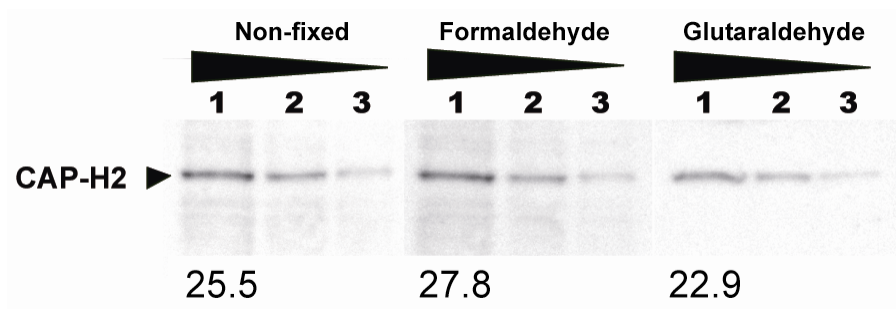


Figure 30

Figure 30. Detection of CAP-H2 signals by Western blotting of cell lysates, which were fixed with glutaraldehyde on the membrane

Increasing quantities of total cell lysates of normal DM cells were loaded into lanes 1–3. CAP-H2 signal values after background subtraction are shown at the bottom. Note that glutaraldehyde did not change the antibody-epitope(s) in the CAP-H2 of the condensin complex.

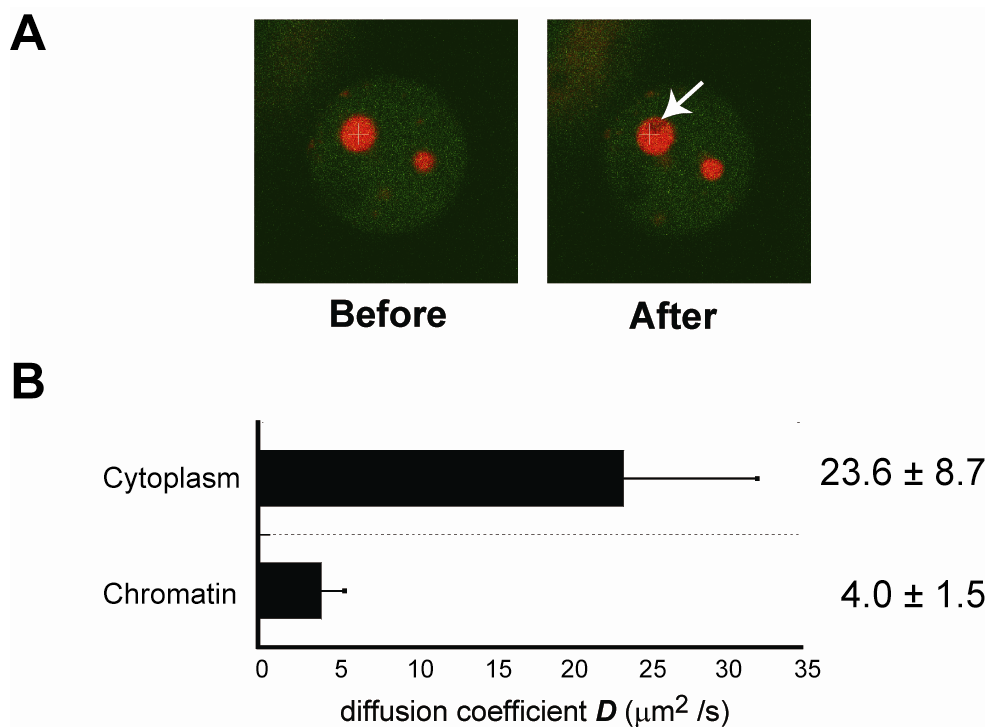


Figure 31

Figure 31. Slower diffusion of EGFP-monomer molecules in apoptotic chromatin

(A) The chromatin of apoptotic cell showed condensed chromatin with a strong H2B-mRFP1 signal. After the FCS measurement, the H2B-mRFP1 signal of the measured region was photobleached out (shown by arrow). (B) Mean D of EGFP-monomer molecules in the apoptotic cytoplasm (upper) and chromatin (lower). For details of the D calculation, see Experimental Procedures. Their mean value and standard deviation (SD) are shown on the right. Note that the value in the cytoplasm was similar to that in the cytoplasm of normal cells.

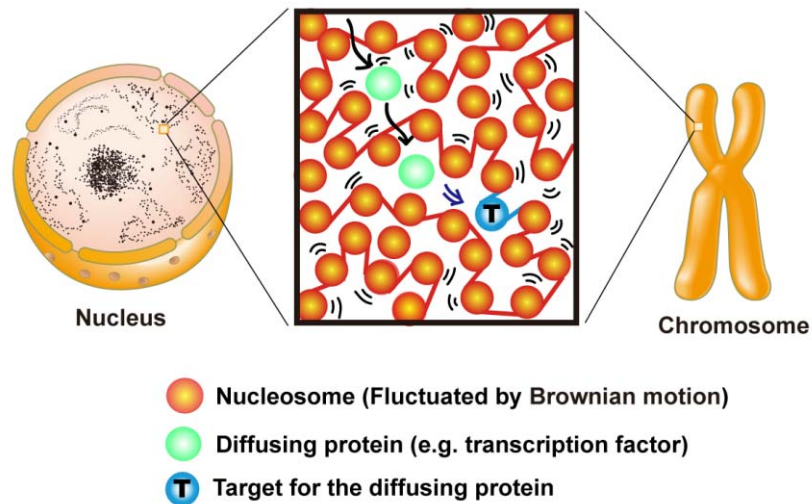


Figure 32

Figure 32. The dynamic local movement of nucleosomes

Interphase chromatin and dense mitotic chromosomes and mitotic chromosomes have comparable protein diffusibility. This diffusibility is allowed by a novel local dynamics of individual nucleosomes. Inhibition of the local dynamics by cross-linking impaired the diffusibility and targeting efficiency in dense chromatin regions (Figure 29). The local movement of nucleosomes is the basis for scanning genome information.

6. EXPERIMENTAL PROCEDURES

6-1. Antibodies

Antibodies (Abs) against H2B (07-371) and H4 (07-108) were obtained from Millipore.

Abs against GFP (598) and RFP (M155-3) were purchased from MBL. Rat monoclonal

Ab against human CAPD-H2 was kindly provided by Dr. Tachibana (Osaka City University).

6-2. Plasmid Construction Expressing H2B-mRFP1 and Tandem EGFP

For constructing $P_{EF-1\alpha}$ -H2B-mRFP, to replace the CMV promoter of pcDNA5/FRT vector (Invitrogen) to EF1-alpha promoter, EF1-alpha promoter region was amplified from pEF5/FRT/V5-DEST vector (Invitrogen) by PCR with a primer sets. The amplified fragment was inserted into pcDNA5/FRT to make pEF1-FRT. The coding regions of human H2B and mRFP1 were amplified from pExPR- pEF1-H2B-mRFP1- pEF1-EGFP with the following primer sets:

5'-CTAGCTAGCATGCCAGAGCCAGCGAAGTCTG-3' and

5'-CCCAAGCTTTTAGGCGCCGGTGGAGTGGCGG-3'. The amplified fragment was digested with *NheI* and *HindIII*, followed by ligation to create pEF1-H2B-mRFP1-FRT.

Plasmids expressing each tandem EGFP_n were synthesized with the plasmid expressing

EGFP-C1 (Clontech, Palo Alto, CA). The EGFP-C1 was excised at the *NdeI* and the *SmaI* restriction sites and ligated between the *NdeI* and *Eco47 III* restriction sites of another EGFP-C1. The linker between EGFP_n containing 25 random amino acid residues (SGLRSRAQASNSAVDGTAGPLPVAT) originated from the remaining bases of the multiple-cloning site.

The human *cdk1* promoter sequence was amplified with the following PCR primer set:

5'-GGCAAGCTTCAGCTGCGCTGGAGGCTGAGGCCGATTGCTTG-3' and

5'-GGCAAGCTTCGGCTTATTATTCCGCGGCGGCCGCAGCGAGC-3'. The

amplified fragment was cut with *HindIII* and ligated into *HindIII*-precut pEF1-H2B-mRFP1-FRT. I named this constructed vector pEF1-H2B-mRFP1-pcdk1-FRT. EGFP₁, EGFP₃, and EGFP₅ were cut out and blunted by T4 DNA polymerase (Toyobo) and inserted into *EcoRV*-precut pEF1-H2B-mRFP1-pcdk1-FRT to obtain pEF1-H2B-mRFP1-pcdk1-EGFP_n-FRT.

6-3. Plasmid Construction Expressing a Low Amount of PA-GFP-H4

pPA-GFP-H4 was kindly provided by Dr. Dirks (Leiden University, The Netherlands).

The plasmid was cut with *NheI* and *BamHI* to cut out the PA-GFP-H4 fragment. This fragment was blunted by T4 DNA polymerase and inserted into an *EcoRV*-precut

pEF5/FRT/SV-DEST Gateway Vector (Invitrogen) to obtain pEF1-PA-GFP-H4-FRT.

6-4. Cell Culture and Isolation of Stable Cell Lines

Indian Muntjac cells (DM cells) were generously gifted from Drs. Kimura and Cook (Osaka University and Oxford University, respectively) (37). The cells were cultured in Dulbecco's modified Eagle's medium (DMEM) supplemented with 15% fetal bovine serum at 37°C in 5% CO₂. For establishment of DM cells stably expressing H2B-mRFP1 and EGFPn ($n = 1, 3, \text{ or } 5$), Flp-In system (Invitrogen) was used. pFRT-bla (56) was first transfected into DM cells using the Effectene transfection reagent kit (Qiagen). Cells containing the FRT site were selected using 5 µg/ml blasticidin S (Invitrogen) and used for isolation of stable transformants. pEF1-H2B-mRFP1-pcdk1-EGFPn-FRT was transfected into DM cells harboring an FRT site and then transformants were selected with 200 µg/ml hygromycin B (Invitrogen) (Figure 5).

6-5. Western Blotting

Western blotting analysis was carried out using the ECL enhanced chemiluminescence detection system (GE Healthcare). Primary antibodies used were anti-EGFP (1:1000),

anti-RFP (1:500), anti-H2B (1:1000), and anti-H4 (1:1000). Secondary antibody was horseradish peroxidase-conjugated antibody (1:2000).

6-6. FCS Measurement and Quantitative Analysis

Live cell imaging was performed using an LSM510 confocal laser microscope (Carl Zeiss, Germany). LSM observations were all performed at 25°C. EGFPn ($n = 1, 3, \text{ or } 5$) was excited at 488 nm with a CW Ar⁺ laser through a water immersion objective lens (C-Apochromat, 40×, 1.2 NA; Carl Zeiss). H2B-mRFP1 was imaged using a 543-nm laser light. To avoid bleed-through effects in double-scanning experiments, EGFP and mRFP1 were scanned independently in a multitracking mode.

FCS measurements were all performed at 25°C on a ConfoCor 2 (Carl Zeiss). Each stable cell line was cultured on LAB-TEK chambered coverslips with eight wells (Nalge Nunc International, Rochester, NY). Before FCS measurement, medium changed from DMEM containing phenol-red to not containing one. Excitation of EGFP was carried out at 488 nm (under 6.3 μW) by adjusting an acousto-optical tunable filter (AOTF) to minimum. All autocorrelation functions were measured for 10 s five times or less at 2-s intervals, since the mitotic chromosome is very slowly moving during the mitotic process, causing nonstationary slow fluorescent fluctuations during long

measurement periods. To obtain diffusion time, the fluorescence autocorrelation curve functions [FAFs; $G(\tau)$] of the measurements were fitted by the following one-component model with or without a triplet term:

$$G(\tau) = 1 + \frac{1}{N} \left(\frac{1}{1 + \tau/\tau_D} \right) \left(\frac{1}{1 + (1/s)^2 (\tau/\tau_D)} \right)^{\frac{1}{2}}$$

where N is the number of molecules in detection volume; τ_D is correlation time; w and z are the width and axial length of the detection volume, respectively; and s is the structure parameter (z/w).

Diffusion times have the following relation to the diffusion coefficient (D):

$$\tau_D = w^2/4D$$

The D of EGFP (τ_{EGFP}) was calculated from the reported value of D of control Rho6G ($D_{Rh6G} = 280 \mu\text{m}^2/\text{s}$), and the measured values of the diffusion times of Rh6G (τ_{Rh6G}) and EGFP (D_{EGFP}), as follows:

$$\frac{D_{EGFP}}{D_{Rh6G}} = \frac{\tau_{Rh6G}}{\tau_{EGFP}}$$

Note that all FAFs from FCS measurements under our conditions were well fit only by the one-component model (Figure 11), perhaps because when the probe molecules are

overexpressed, some become immobilized. This immobilized fraction tends to be easily photobleached, and consequently generate an apparent “slow diffusional component” with FCS measurements (Pack *et al.*, 2006). However, the DM cells stably expressed EGFP probe molecules at a very low level; thus, almost no immobilized probe fraction would exist, and so no “slow diffusional component.”

6-7. Nucleosome Concentrations in DM Cells

To measure nuclear and chromosomal volumes, z-stack images were acquired by LSM510 microscopy after staining with TO-PRO-3 (Invitrogen). Chromatin regions were segmented from the image stacks using a novel method. Chromatin regions in the image stack have variable signal intensities and background noises, making them difficult to distinguish. To detect the correct chromatin region, I developed an image processing framework based on the following three simple methods, which analyze the image features characterizing the target objects: the mean shift filtering (Comaniciu and Meer, 2002), the k-means algorithm (MacQueen, 1967), and the closing operator (Jones and Svalbe, 1994). Each nuclear or chromosome volume was calculated from the segmented areas.

To calculate the nucleosome number, I supposed the genome size of Indian Muntjac

cells (DM cells) to be 2.1×10^9 bp (Johnston *et al.*, 1982) and that the nucleosome spacing was ~ 200 bp (Kornberg and Lorch, 1999). Since I found that the chromosome number increased by 1.5-fold in DM cells, I estimated that the total nucleosome number was $\sim 3 \times 10^7$ /diploid DM cell. The nucleosome concentration was obtained using the total nucleosome number and the measured nuclear or chromosome volumes.

6-8. Metropolis Monte Carlo Simulation of Nucleosomes and EGFP-pentamers

All molecules were represented as spherical hardbodies. Diffusive motions of the molecules were calculated using the Metropolis Monte Carlo method without long-range potentials (Morelli and ten Wolde, 2008). The diameter and D of nucleosomes (red balls) and EGFP-pentamers (green balls) used in the simulations were 10.3 nm, $8.68 \mu\text{m}^2/\text{s}$, 12.8 nm, and $7.00 \mu\text{m}^2/\text{s}$, respectively. These values were obtained as follows: the red ball representing a nucleosome was determined to have an equivalent volume to that of a nucleosome structure (Luger *et al.*, 1997). The D of nucleosomes (red balls) was obtained using the Stokes–Einstein relation based on the diameter and D of EGFP-monomers measured in the cytoplasm (3.80 nm and $23.5 \mu\text{m}^2/\text{s}$, respectively). The diameter of EGFP-pentamers was also obtained using the same relation from the D obtained by FCS measurements.

Simulations were conducted in a cubic box of size 149 nm with periodic boundaries. One-hundred EGFP-pentamers and 200 or 1000 nucleosomes (corresponding to 0.1 mM or 0.5 mM, respectively) were placed randomly. Results were obtained by averaging 1000 samples from 10 independent trials. Simulation time step was 1 ns. Similar results with a smaller time step (0.1 ns) confirmed the simulation convergence. The “dog on a leash” model does not allow nucleosomes to displace more than a defined distance from their initial positions at $t = 0$ s.

6-9. Biochemical Characterization of Nucleosomes Containing PA-GFP-Histone H4

For isolation of nuclei, I followed the method of Ura et al. (Ura and Kaneda, 2001). Wash the cell pellet by gentle resuspension in ice-cold PBS and centrifugation at 500g for 10 min at 4°C. After that, wash the cell pellet again with ice-cold nuclei isolation buffer [10 mM Tris-HCl pH 7.5, 1.5 mM MgCl₂, 1 mM CaCl₂, 0.25 M sucrose and 0.1 mM PMSF] and resuspended the cell pellet in ice-cold nuclei isolation buffer plus 0.5% Triton X-100. This pellet was left on ice for 10 min to swell. The swollen cells were homogenized on ice with Dounce homogenizer. The homogenized cells were centrifuged at 500g for 5 min at 4°C. The supernatants was discarded and the nuclear pellet was resuspended with nuclei isolation buffer. This procedure was repeated until

the nuclei were pure white.

To make oligonucleosomes, isolated nuclei were treated with micrococcal nuclease at a concentration of 5 units/ μ l (Worthington) for 10 min at 35°C. After dialysis in a buffer [0.2 M NaCl, 10 mM Tris-HCl (pH7.5), 1 mM EDTA, 0.1 mM PMSF], the digested nucleosome solution was loaded on the HTP column (Bio-Rad). The elution was performed in a stepwise manner: the first elution buffer [10 mM Tris-HCl (pH 7.5), 1 mM EDTA, 0.1 mM PMSF] containing 1 M NaCl dissociated mainly histones H2A and H2B. Histones H3 and H4 came out with the second buffer containing 2 M NaCl. Each elution fraction was concentrated by trichloroacetic acid precipitation and used for CBB staining and Western blotting.

6-10. Visualization of Single Nucleosome Motion in Mammalian Living Cells

A homemade optical setup with a fluorescence microscope (TE 2000-E: Nikon) (Tani *et al.*, 2005) was used to observe the distribution of single PA-GFP-H4 molecules expressed in DM cells. Light from a 20 mW 488-nm diode-pumped solid-state laser was introduced into the microscope through an optical path installed on a vibration insulation table. Two neutral density filters and an electromagnetic shutter were placed in the optical path. Through an objective lens (100 \times PlanApo TIRF, NA 1.49; Nikon),

DM cells grown on a glass coverslip were exposed to the excitation light. The incident angle of the laser beam to the specimen plane was chosen so as to obtain a highly inclined plane illumination (HILO system, (Tokunaga *et al.*, 2008)). Collected fluorescence from the cells was focused on the electron-multiplied CCD camera (Andor Technology, UK). The observation stage was kept at a constant 37°C. For imaging of PA-GFP, interference filters were used. The length of a side of a single pixel corresponded to 40 nm on the specimen plane.

Sub-pixel-accuracy positions of PA-GFP dots were determined using the image processing software PolyParticleTracker (Rogers *et al.*, 2007). The accuracy for determining the position of fluorescent dots was estimated using the FIONA method (Thompson *et al.*, 2002; Yildiz *et al.*, 2003; Ober *et al.*, 2004). With this procedure, the trajectory of each fluorescent dot was obtained. I calculated the displacement and the MSD of fluorescent nucleosomes from the tracking data (857 points from eight cells in interphase, 844 points from 12 cells in mitosis, 37 points from eight cells fixed with 2% glutaraldehyde, and 100 points from fluorescence beads). The originally calculated MSD was in two-dimensions. To obtain the three-dimensional value, the two-dimensional value was multiplied by 1.5 ($4Dt \rightarrow 6Dt$). Using KaleidaGraph (Synergy Software, USA), histograms of the displacement were prepared.

PA-GFP-histone H4 has some flexible regions, including the linker and histone tail, which is maximally 50 amino acid residues, corresponding to ~17 nm long. I observed by FCS rapid movement of free GFP in the chromosomes at $15 \mu\text{m}^2/\text{s}$. If PA-GFP is rapidly mobile within a restricted area like a “dog on a leash,” I considered that the effect of the flexible region on the nucleosome position determination is negligible.

6-11. Metaphase Spread Staining and Western Blotting with Condensin Antibody

Metaphase spreads were prepared from mitotic DM cells, which were collected by mitotic shake-off, swollen in 75 mM KCl for 15 min, and then spread on slides using a cytocentrifuge. The spreads were fixed in 2% paraformaldehyde or 2% glutaraldehyde in HMK buffer [20 mM Hepes (pH 7.5), 1 mM MgCl₂, 100 mM KCl] for 15 min at room temperature and then treated with 0.2% triton X-100 in HMK for 5 min. Another spread was not fixed and directly treated with 0.2 % triton X-100 in HMK for 5 min. Only the spread fixed with glutaraldehyde was washed with 1 mg/ml sodium borohydride in HMK for 10 min to quench unreacted aldehyde, which somehow produced a strong autofluorescence signal. Each chromosome spread was incubated with a 200-fold-diluted rat monoclonal antibody against CAP-H2 (a condensin II subunit) and 1% NGS in HMK buffer at room temperature for 2 hr. After extensive

washing with HMK buffer, they were incubated with 1000-fold-diluted anti-rat Alexa594-labeled goat IgG and 1% NGS in HMK buffer at room temperature for 1 hr. After extensive washing with HMK buffer, they were incubated with DAPI in MilliQ water at room temperature for 5 min and after washing, the chromosomes were mounted in PPDI [10 mM HEPES pH 7.7, 2 mM MgCl₂, 100 mM KCl, 5 mM EGTA, 78% glycerol and 1 mg/ml paraphenylene diamine] and the coverslips were sealed with manicule.

All images were acquired with wide-field fluorescence microscope (Nikon) using a water immersion objective lens (Plan Apo, 60×, 1.2NA; Olympus). Total cell lysates from normal DM cells were electrophoresed on 8% polyacrylamide gels and transferred to Immobilon-P PVDF membranes (Millipore). The membrane was then fixed with formaldehyde or glutaraldehyde and then subjected to Western blotting with rat monoclonal antibody against CAP-H2 (a condensin II subunit). A quantitative analysis was carried out using Image J (NIH).

7. ACKNOWLEDGEMENTS

This research would not have been possible without the help of so many people.

I would like to express my deepest gratitude to my super advisor, Prof. Kazuhiro Maeshima, for his excellent guidance, caring, and providing me with original philosophy for doing research. His attitude for science inspires my feeling of respect.

I would like to thank Dr. Pack (RIKEN) and Prof. Kinjo (Hokkaido University) for FCS support, and Dr. Takemoto and Dr. Yokota (RIKEN) for help of image analysis using VCAT systems, and Dr. Kaizu and Dr. Takahashi (RIKEN) for nucleosome simulation, and Dr. Hanafusa (Maeshima lab), Dr. Tani (MBL), Dr. Sako (RIKEN) and Prof. Nagai (Osaka University) for single molecule support, advice and discussion.

It is a pleasure to thank everyone in Maeshima lab. I appreciate Dr. Hiratani, Dr. Takata and Dr. Hanafusa for helpful discussion, and Dr. Kumagai, F. Kamada, K. Hamasuna, and S. Tamura for technical assistance.

I thank Dr. Kimura (Osaka University), Dr. Yahata (Nagasaki University) and Dr. Tachibana (Osaka City University) for providing their materials.

Finally, I would like to thank my family and members of Murata lab (The University of Tokyo) for encouraging me.

8. References

Alberts, B., Johnson, A., Lewis, J., Raff, M., Roberts, K., and Walter, P. (2007).
Molecular Biology of the Cell, Fifth Edition.

Bancaud, A., Huet, S., Daigle, N., Mozziconacci, J., Beaudouin, J., and Ellenberg, J.
(2009). Molecular crowding affects diffusion and binding of nuclear proteins in
heterochromatin and reveals the fractal organization of chromatin. *Embo J* 28,
3785-3798.

Belmont, A.S., Li, G., Sudlow, G., and Robinett, C. (1999). Visualization of large-scale
chromatin structure and dynamics using the lac operator/lac repressor reporter system.
Methods Cell Biol 58, 203-222.

Bloomfield, V.A. (1996). DNA condensation. *Curr Opin Struct Biol* 6, 334-341.

Boonyaratanakornkit, B.B., Park, C.B., and Clark, D.S. (2002). Pressure effects on
intra- and intermolecular interactions within proteins. *Biochim Biophys Acta* 1595,
235-249.

Bouchet-Marquis, C., Dubochet, J., and Fakan, S. (2006). Cryoelectron microscopy of
vitrified sections: a new challenge for the analysis of functional nuclear architecture.
Histochem Cell Biol 125, 43-51.

Chen, D., Dundr, M., Wang, C., Leung, A., Lamond, A., Misteli, T., and Huang, S.

- (2005). Condensed mitotic chromatin is accessible to transcription factors and chromatin structural proteins. *J Cell Biol* 168, 41-54.
- Chubb, J.R., Boyle, S., Perry, P., and Bickmore, W.A. (2002). Chromatin motion is constrained by association with nuclear compartments in human cells. *Curr Biol* 12, 439-445.
- Comaniciu, D., and Meer, P. (2002). Mean Shift: A Robust Approach toward Feature Space Analysis. *IEEE Trans on PAMI* 24, 603-619.
- Cremer T, Markaki Y, Hübner B, Zunhammer A, Strickfaden H, Beichmanis S, Heß M, Schermelleh L, Cremer M, and C, C. (2011). Chromosome Territory Organization within the Nucleus. *Encyclopedia of Molecular Cell Biology and Molecular Medicine*
- Davey, C.A., Sargent, D.F., Luger, K., Maeder, A.W., and Richmond, T.J. (2002). Solvent mediated interactions in the structure of the nucleosome core particle at 1.9 a resolution. *J Mol Biol* 319, 1097-1113.
- Dross, N., Spriet, C., Zwerger, M., Muller, G., Waldeck, W., and Langowski, J. (2009). Mapping eGFP oligomer mobility in living cell nuclei. *PLoS One* 4, e5041.
- Eltsov, M., Maclellan, K.M., Maeshima, K., Frangakis, A.S., and Dubochet, J. (2008). Analysis of cryo-electron microscopy images does not support the existence of 30-nm chromatin fibers in mitotic chromosomes in situ. *Proc Natl Acad Sci U S A* 105,

19732-19737.

Finch, J.T., and Klug, A. (1976). Solenoidal model for superstructure in chromatin. *Proc Natl Acad Sci U S A* 73, 1897-1901.

Frank, J. (2006). Three-Dimensional Electron Microscopy of Macromolecular Assembly.

Fussner, E., Ching, R.W., and Bazett-Jones, D.P. (2011). Living without 30nm chromatin fibers. *Trends Biochem Sci* 36, 1-6.

Gerlich, D., Hirota, T., Koch, B., Peters, J.M., and Ellenberg, J. (2006). Condensin I stabilizes chromosomes mechanically through a dynamic interaction in live cells. *Curr Biol* 16, 333-344.

Gorisch, S.M., Wachsmuth, M., Toth, K.F., Lichter, P., and Rippe, K. (2005). Histone acetylation increases chromatin accessibility. *J Cell Sci* 118, 5825-5834.

Griffiths, G. (1993). Fine structure immunocytochemistry.

Heun, P., Laroche, T., Shimada, K., Furrer, P., and Gasser, S.M. (2001). Chromosome dynamics in the yeast interphase nucleus. *Science* 294, 2181-2186.

Hinde, E., Cardarelli, F., Digman, M.A., Kershner, A., Kimble, J., and Gratton, E. (2011). The impact of mitotic versus interphase chromatin architecture on the molecular flow of EGFP by pair correlation analysis. *Biophys J* 100, 1829-1836.

- Hirano, T. (2005). Condensins: organizing and segregating the genome. *Curr Biol* 15, R265-275.
- Jakob, B., Splinter, J., Durante, M., and Taucher-Scholz, G. (2009). Live cell microscopy analysis of radiation-induced DNA double-strand break motion. *Proc Natl Acad Sci U S A* 106, 3172-3177.
- Johnston, F.P., Church, R.B., and Lin, C.C. (1982). Chromosome rearrangement between the Indian muntjac and Chinese muntjac is accompanied by a deletion of middle repetitive DNA. *Can J Biochem* 60, 497-506.
- Jones, R., and Svalbe, I. (1994). Algorithms for the Decomposition of Gray-Scale Morphological Operations. *IEEE Trans on PAMI* 16, 581-588.
- Kimura, H., and Cook, P.R. (2001). Kinetics of core histones in living human cells: little exchange of H3 and H4 and some rapid exchange of H2B. *J Cell Biol* 153, 1341-1353.
- Kornberg, R.D., and Lorch, Y. (1999). Twenty-five years of the nucleosome, fundamental particle of the eukaryote chromosome. *Cell* 98, 285-294.
- Levi, V., and Gratton, E. (2008). Chromatin dynamics during interphase explored by single-particle tracking. *Chromosome Res* 16, 439-449.
- Levi, V., Ruan, Q., Plutz, M., Belmont, A.S., and Gratton, E. (2005). Chromatin

- dynamics in interphase cells revealed by tracking in a two-photon excitation microscope. *Biophys J* 89, 4275-4285.
- Lippincott-Schwartz, J., and Patterson, G.H. (2009). Photoactivatable fluorescent proteins for diffraction-limited and super-resolution imaging. *Trends Cell Biol* 19, 555-565.
- Losada, A., and Hirano, T. (2005). Dynamic molecular linkers of the genome: the first decade of SMC proteins. *Genes Dev* 19, 1269-1287.
- Luger, K., Mader, A.W., Richmond, R.K., Sargent, D.F., and Richmond, T.J. (1997). Crystal structure of the nucleosome core particle at 2.8 Å resolution. *Nature* 389, 251-260.
- MacQueen, J. (1967). Some Methods for classification and Analysis of Multivariate Observations. *Proc of 5-th Berkeley Symposium on Mathematical Statistics and Probability*, Berkeley, University of California Press, 281-297.
- Maeshima, K., and Eltsov, M. (2008). Packaging the genome: the structure of mitotic chromosomes. *J Biochem (Tokyo)* 143, 145-153.
- Maeshima, K., Hihara, S., and Eltsov, M. (2010a). Chromatin structure: does the 30-nm fibre exist in vivo? *Curr Opin Cell Biol* 22, 291-297.
- Maeshima, K., Hihara, S., and Takata, H. (2010b). New insight into the mitotic

- chromosome structure: irregular folding of nucleosome fibers without 30-nm chromatin fiber. *Cold Spring Harb Symp Quant Biol* 75, 439-444.
- Manders, E.M., Kimura, H., and Cook, P.R. (1999). Direct imaging of DNA in living cells reveals the dynamics of chromosome formation. *J Cell Biol* 144, 813-821.
- Morelli, M.J., and ten Wolde, P.R. (2008). Reaction Brownian dynamics and the effect of spatial fluctuations on the gain of a push-pull network. *J Chem Phys* 129, 054112.
- Nishino, Y., Eltsov, M., Joti, Y., Ito, K., Takata, H., Takahashi, Y., Hihara, S., Frangakis, A.S., Imamoto, N., Ishikawa, T., et al. (2012). Human mitotic chromosomes consist predominantly of irregularly folded nucleosome fibres without a 30-nm chromatin structure. *Embo J* 31, 1644-1653.
- Ober, R.J., Ram, S., and Ward, E.S. (2004). Localization accuracy in single-molecule microscopy. *Biophys J* 86, 1185-1200.
- Olins, D.E., and Olins, A.L. (2003). Chromatin history: our view from the bridge. *Nat Rev Mol Cell Biol* 4, 809-814.
- Pack, C., Saito, K., Tamura, M., and Kinjo, M. (2006). Microenvironment and effect of energy depletion in the nucleus analyzed by mobility of multiple oligomeric EGFPs. *Biophys J* 91, 3921-3936.
- Robinett, C.C., Straight, A., Li, G., Willhelm, C., Sudlow, G., Murray, A., and Belmont,

- A.S. (1996). In vivo localization of DNA sequences and visualization of large-scale chromatin organization using lac operator/repressor recognition. *J Cell Biol* 135, 1685-1700.
- Rogers, S.S., Waigh, T.A., Zhao, X., and Lu, J.R. (2007). Precise particle tracking against a complicated background: polynomial fitting with Gaussian weight. *Phys Biol* 4, 220-227.
- Sandin, S., Ofverstedt, L.G., Wikstrom, A.C., Wrangé, O., and Skoglund, U. (2004). Structure and flexibility of individual immunoglobulin G molecules in solution. *Structure* 12, 409-415.
- Straight, A.F., Belmont, A.S., Robinett, C.C., and Murray, A.W. (1996). GFP tagging of budding yeast chromosomes reveals that protein-protein interactions can mediate sister chromatid cohesion. *Curr Biol* 6, 1599-1608.
- Strick, R., Strissel, P.L., Gavrillov, K., and Levi-Setti, R. (2001). Cation-chromatin binding as shown by ion microscopy is essential for the structural integrity of chromosomes. *J Cell Biol* 155, 899-910.
- Tani, T., Miyamoto, Y., Fujimori, K.E., Taguchi, T., Yanagida, T., Sako, Y., and Harada, Y. (2005). Trafficking of a ligand-receptor complex on the growth cones as an essential step for the uptake of nerve growth factor at the distal end of the axon: a

- single-molecule analysis. *J Neurosci* 25, 2181-2191.
- Tavormina, P.A., Come, M.G., Hudson, J.R., Mo, Y.Y., Beck, W.T., and Gorbsky, G.J. (2002). Rapid exchange of mammalian topoisomerase II alpha at kinetochores and chromosome arms in mitosis. *J Cell Biol* 158, 23-29.
- Thompson, R.E., Larson, D.R., and Webb, W.W. (2002). Precise nanometer localization analysis for individual fluorescent probes. *Biophys J* 82, 2775-2783.
- Tokunaga, M., Imamoto, N., and Sakata-Sogawa, K. (2008). Highly inclined thin illumination enables clear single-molecule imaging in cells. *Nat Methods* 5, 159-161.
- Ura, K., and Kaneda, Y. (2001). Reconstitution of chromatin in vitro. *Methods Mol Biol* 181, 309-325.
- Vazquez, J., Belmont, A.S., and Sedat, J.W. (2001). Multiple regimes of constrained chromosome motion are regulated in the interphase *Drosophila* nucleus. *Curr Biol* 11, 1227-1239.
- Wachsmuth, M., Caudron-Herger, M., and Rippe, K. (2008). Genome organization: balancing stability and plasticity. *Biochim Biophys Acta* 1783, 2061-2079.
- Wiesmeijer, K., Krouwels, I.M., Tanke, H.J., and Dirks, R.W. (2008). Chromatin movement visualized with photoactivable GFP-labeled histone H4. *Differentiation* 76, 83-90.

Woodcock, C.L., Frado, L.L., and Rattner, J.B. (1984). The higher-order structure of chromatin: evidence for a helical ribbon arrangement. *J Cell Biol* 99, 42-52.

Yildiz, A., Forkey, J.N., McKinney, S.A., Ha, T., Goldman, Y.E., and Selvin, P.R. (2003). Myosin V walks hand-over-hand: single fluorophore imaging with 1.5-nm localization. *Science* 300, 2061-2065.

Yoshikawa, K., and Yoshikawa, Y. (2002). Compaction and Condensation of DNA. 137-163.